Characterization of the Rapid Gas Decompression Behavior of HNBR Based Rubber

Master Thesis

by

Bernd Schrittesser

submitted to the

Institute of Materials Science and Testing of Plastics
University of Leoben

prepared at the

Polymer Competence Center Leoben GmbH

Thesis Supervisor: Dipl.-Ing. Dr.mont. Zoltán Major

Academic Advisor: Univ.-Prof. Dipl.-Ing. Dr.mont. Gerald Pinter

Leoben, June 2010

Affidavit

I declare in lieu of oath that I wrote this thesis and performed the associated research myself, using only literature cited in this volume.

---------- ----------

Date Signature

Acknowledgment

I thank Univ.-Prof. Dipl.-Ing. Dr.mont. Gerald Pinter, interim Head of the Institute of Materials Science and Testing of Plastics, for his appraisal as academic supervisor.

Furthermore, I thank my supervisor and friend Dipl.-Ing. Dr.mont. Zoltán Major for his help and all the opportunities he offered me. Without his help, I wouldn't have been able to perform my research work the way I did. I learned a lot from him and I thank him for everything.

Very special thanks go to SKF ECONOMOS Austria GmbH, in particular Dipl.-Ing. Dr.mont. Thomas Schwarz as well as Dipl.-Ing. Mario Mitterhuber and Dipl.-Ing. Manfred Moitzi for the supply of the experimental materials.

Appreciation is (also) extended to Dipl.-Ing. Dr. Laszlo Olah and Dipl.-Ing. Daniel Tscharnuter for efficient discussions and new thoughts as well as new ideas for experiments and test setups. Furthermore, I would like to thank Dipl.-Ing. Andreas Hausberger, Dipl.-Ing. Peter Fuchs and Simon Gastl, my work colleagues and the whole PCCL team for the loyal working environment.

I would also like to thank my family, especially my mother, who gave me the opportunity to study. Moreover, I thank them for their backing and support in all circumstances.

The research work of this thesis was performed at the Polymer Competence Center Leoben GmbH (PCCL, Austria) within the framework of the COMET-program of the Austrian Ministry of Traffic, Innovation and Technology with contributions by the Institute of Materials Science and Testing of Plastics at the University of Leoben and the SKF ECONOMOS Austria GmbH. The PCCL is funded by the Austrian Government and the State Governments of Styria and Upper Austria.

Abstract

Seals and hoses for oilfield applications are exposed to high temperatures, aggressive fluids and various gases. A specific failure, the rapid gas decompression failure, can occur during the exposure to high pressure and various gases. This failure results in crack growth, extensive deformation, swelling, blisters and in some cases catastrophic fragmentation of the vulcanised rubber.

The aim of this thesis was to provide additional information on the rapid gas decompression failure. This information is relevant, because of the unique thermal and mechanical properties as a result of the penetration of the ambient gas. According to several engineering standards, unconstrained and constrained measurements are common (NACE and NORSOK). In these standards the failure interpretation is solely based on the visual observation after the test. Therefore, additional measurements are necessary to understand the material performance during the exposure to high pressure gas. In the first step in a former thesis a camera system was implemented in order to observe the volume change during the test procedure. In this thesis the test set-up was adapted for in situ constrained tests and the measurement of uniaxial expansion forces in the tested materials.

Four hydrogenated nitrile butadiene formulations with different acrylonitrile content and fillers were investigated. Based on the recorded measurements, a clear correlation between unconstrained and constrained measurements was found. To characterize the filler dependent behavior and to investigate the influence of the rising acrylonitrile content a filler factor and an acrylonitrile factor were defined. A clear effect of ACN and filler content was found in both test set-ups. In particular, different incubation times were observed for the volume change and force increase during depressurization. Additional tests, including relaxation test, dynamic mechanical analyses, thermal conductivity and expansion measurements were carried out to supply fundamental material properties. The temperature-dependent storage modulus seems to influence the investigated volume increase during depressurization. With rising storage modulus, the volume change drops and vice versa.

Zusammenfassung

Dichtungen und Schläuche sind in speziellen Anwendungsgebieten der Erdölindustrie hohen Temperaturen, aggressiven Flüssigkeiten und verschiedenen Gasgemischen ausgesetzt. Betrachtet man den Spezialfall der Kombination des hohen Druckes mit aggressiven Gasen kann ein spezieller Versagensfall, das „Rapid Gas Decompression“-Versagen auftreten. Dieser Fehler verursacht Risswachstum, hohe Deformation, Blasenbildung und in einigen Fällen eine katastrophale Fragmentierung der eingesetzten Dichtungswerkstoffe.

Ziel dieser Arbeit war es, zusätzliche Information über das „Rapid Gas Decompression“-Versagen zu sammeln. Aufgrund der einmaligen thermischen und mechanischen Eigenschaften, die während der Penetration des Gases auftreten, ist speziell dieser Aspekt sehr relevant. In Bezug auf industriell eingesetzte Normen (NORSOK und NACE) werden die freie Volumenänderung sowie die Volumenänderung unter Zwangsbedingungen charakterisiert. Basierend auf diesen Normen erfolgt die Fehlerinterpretation visuell am geprüften Prüfkörper. Um die Materialeigenschaften während der Gasbelastung zu erfassen, sind jedoch zusätzliche Messungen notwendig. Der erste Schritt war die Implementierung eines Kamerasystems, mit dem die Volumenänderung während des Versuches erfasst werden konnte. Diese Arbeit beschreibt die Implementierung eines in-situ Prüfstandes, um die uniaxiale Expansionskraft der Testmaterialien aufzuzeichnen.

Vier hydrierte nitrilbutadienkautschuk Formulierungen mit unterschiedlichem Acrylnitril-Gehalt und verschiedenen Füllstoffen wurden untersucht. Durch die Vielzahl an Messungen zeigte sich eine eindeutige Korrelation zwischen freier Volumen-Expansion und Expansion unter Zwangsbedingungen. Um das füllstoffabhängige Verhalten und den Einfluss des steigenden Acrylnitril-Gehalts zu erfassen wurden ein Füllstofffaktor und ein Acrylnitrilfaktor gebildet. Die Variierung der Materialeigenschaften ermöglichte die Erfassung des Einflusses unterschiedlicher Acrylnitril-Konzentrationen und Füllstoffsysteme. Zusätzlich wurden abweichende Inkubationszeiten für die Volumenänderung und den Kraftanstieg aufgezeichnet. Weitere Versuche, wie Relaxationsexperimente, dynamisch mechanische Analysen, Messungen der thermischen Leitfähigkeit sowie der thermischen Ausdehnung dienten der Erfassung zusätzlicher

Materialeigenschaften. Das temperaturabhängige Speichermodul zeigte eine Korrelation zu der beobachteten Volumenänderung während der Entlastungsphase. Mit steigendem Speichermodul verringerte sich die Volumenszunahme und umgekehrt.

Table of Contents

1 INTRODUCTION AND OBJECTIVES

Elastomer components (seal and hoses) for oilfield applications have to withstand high temperatures, different aggressive fluids and variations of gas. A specific failure, the rapid gas decompression failure, can occur during the exposure to high pressure and various gases. This failure may cause internal cracking, extensive deformation, swelling, blisters and in some cases catastrophic fragmentation of the vulcanised rubber. Discussions of the failure behavior started in the late 50s [Gent and Lindley, 1958] and still persist [Briscoe, 1994, Hertz, 1996, Major and Lang, 2009].

This master thesis presents a part of a large-scale research project on the applicability of elastomers for oilfield applications. The project was realized by the Polymer Competence Center Leoben GmbH (PCCL) in cooperation with SKF Economos GmbH.

The characterization of the rapid gas decompression behavior was dealt with in the master thesis by Klaus Lederer [Lederer, 2006]. The goal of Klaus Lederer's thesis was to implement an optical test set-up for instrument measurements. Furthermore, the influence of multi-cycle pressurization/depressurization was investigated. Additionally to RGD measurements, a comprehensive fracture mechanics test series with different specimens and test configurations was performed. In Figure 1.1 a short overview of previous and future measurements is depicted.

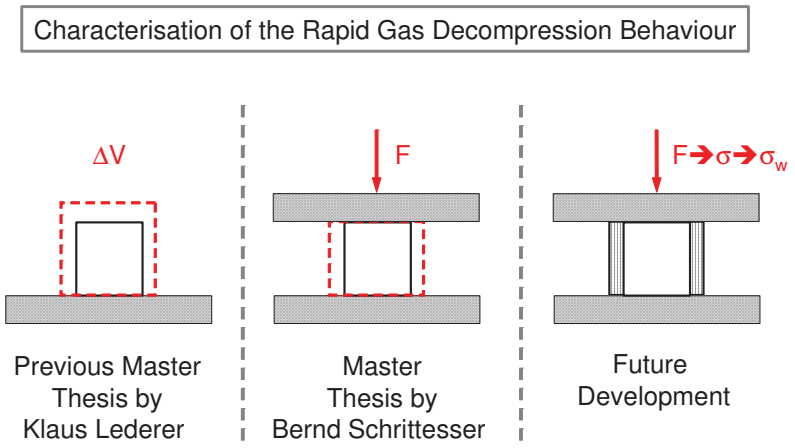

Figure 1.1: Project overview

Due to the importance of the constrained measurements, the first objective of this thesis was to implement an instrumented relaxation test system. For the realization, a novel measurement system was implemented to record the force during the compression and decompression phase.

The second objective was the implementation of the material characterization with different test set-ups. Therefore, instrumented unconstrained tests with optical measurement systems were carried out and compared with the new instrumented constrained test set-up. Moreover, the instrumented relaxation test set-up was compared with the monotonic uniaxial relaxation test of an INSTRON universal testing system.

2 BASIC CONSIDERATIONS

2.1 Elastomers for oilfield applications

A high variation of processes and methods for on-shore and off-shore applications makes it difficult for a material engineer to develop the correct material. Furthermore, complications like high temperatures/pressure and different fluids hinder the selection and have to be considered.

General material requirements for elastomers used in oilfield applications are chemical capability, low and high temperature resistance (up to 200°C), very good mechanical properties, low friction and long life. Basically, 5 materials are used for such an appliance, nitrile butadien rubber (NBR), hydrogenated nitrile butadien rubber (H-NBR), fluoroelastomer (FKM/FPM), terfluoroethylene/propylene copolymers (TFE/P) and perfluoroelastomers (FFKM) [Walker, 2009].

Nitrile butadiene rubber, NBR

Nitrile butadiene rubber has a wide range of use. Different grades of NBR are produced in the emulsion copolymerisation of butadiene and acrylonitrile. The basic differences between the grades are the acrylonitrile content, the vulcanisation temperature and the mooney viscosity. The acrylonitrile content is the most important property, influencing the glass transition temperature, oil resistance and cold flexibility. This material is limited to weathering resistance with the modest temperature resistance of -30°C to 120°C [Walker, 2009].

Hydrogenated nitrile butadien rubber, H-NBR

H-NBR is manufactured out of NBR where no more carbon double bonds in the main chain exist. This state is reached through hydrogenation. Excellent oil/fuel resistance of NBR with distinguished mechanical properties (e.g. tearing strength, modulus, abrasion) makes this material suitable for the use in RGD – applications, although it is limited in resistance to aromatics. Moreover, a better chemical resistance, weatherability, thermal capability (-40°C to 180°C) and very good abrasion resistance qualifies H-NBR for oil and gas field applications [Walker, 2009].

Fluoroelastomer, FKM/FPM

Fluoroelastomers have excellent resistance to oil-, fuel-, mineral-, synthetic - lubricants, aliphatic/aromatic hydrocarbons and many mineral acids. The thermal and chemical resistance depends on the fluorine level and cure system. Moreover, FKM is limited by resistance to steam, hot water and other polar fluids with a theoretical temperature application range from -20°C to 230°C [Walker, 2009].

Tetrafluoroethylene/propylene copolymers, TFE/P

Outstanding ozone/weathering resistance combined with projecting resistance to steam adding the best radiation resistance of all elastomers, characterizes this material. Furthermore, TFE/P shows good heat (0°C to 200°C, in steam: 260°C) and overall chemical resistance. Limitations for TFE/P are the high compression set, the high glass transition temperature and the difficult manufacturing process [Walker, 2009].

Perfluoroelastomers, FFKM

For FFKM, the ultimate performance considering chemical and heat resistance is reached. The only limitations for this elastomer are the modest mechanical properties as well as a high price. The limitation of use concerning the temperature ranges from -25°C to 315°C [Walker, 2009].

For the specific application in chokes and valves or in blowout preventers, H-NBR seems to be the best material. Moreover, H-NBR shows the best resistance regarding the rapid gas decompression failure against sour gas and high CO_2. Due to these aspects, H-NBR is used for further analyses.

2.1.1 Nitrile butadiene rubber (NBR)

Today NBR is the 7th most manufactured elastomer worldwide. Nitrile Butadiene Rubber is produced by means of the radical copolymerisation of butadiene and acrylonitrile in liquid emulsion. Basically, NBR can be fabricated with each acrylonitrile (ACN) – content, generally a content of 15 – 50wt% is used. To avoid chain branching, the conversion is stopped at 70 – 80%, using sodium

hydrosulphide. For the crosslinking reaction, a sulphur activator or a peroxide system is required. The peroxide system provides a higher thermal stability and a smaller compression set [Sommer and Röthemeyer, 2006].

Vulcanised rubber properties general depend on the ACN content, the micro structure and the macro structure.

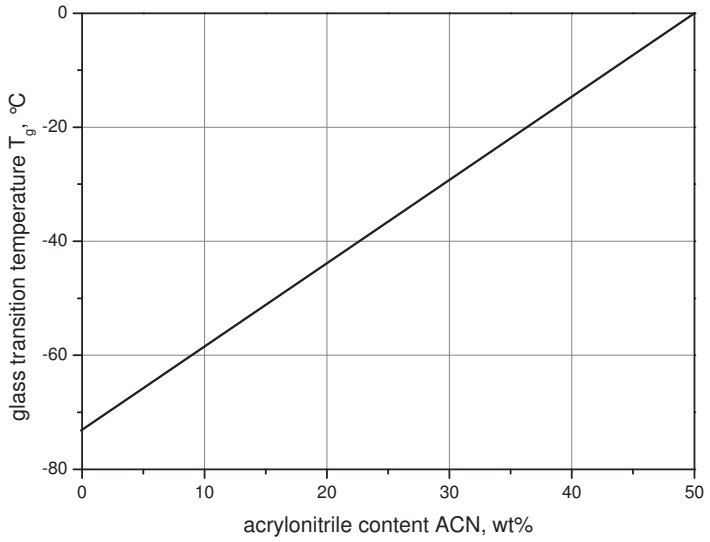

Figure 2.1: Influence of the acrylonitrile content on the glass transition temperature [Sommer and Röthemeyer, 2006]

Table 2.1: Influence of the acrylonitrile content on the properties of the vulcanised rubber [Sommer and Röthemeyer, 2006]

Properties	ACN content rising from 18% to 48%
Fuel and oil resistance	↑
Gas permeability	↓
Flexibility at low temperatures	↓
Density, modulus, hardness	↑
Tear strength	↑
Elasticity	↓
Compression set	↑
Abrasion resistance	↑
Ageing resistance	↑

This rubber is amorphous without any strain crystallization effect. As depicted in Figure 2.1, the acrylonitrile content hardly influences the glass transition

temperature. With rising ACN content the oil resistance and gas proofness build up, however properties depend on the glass transition temperature, e.g. damping, elasticity and the flexibility at low temperatures are influenced negatively (Table 2.1).

Due to the inexistent strain crystallization, active fillers with reinforcing properties are necessary. Mainly, carbon black and brightness fillers are common. Carbon black is used to improve the process ability and mechanical properties. Non-black fillers, such as silicic acid, offer a higher tear growth resistance.

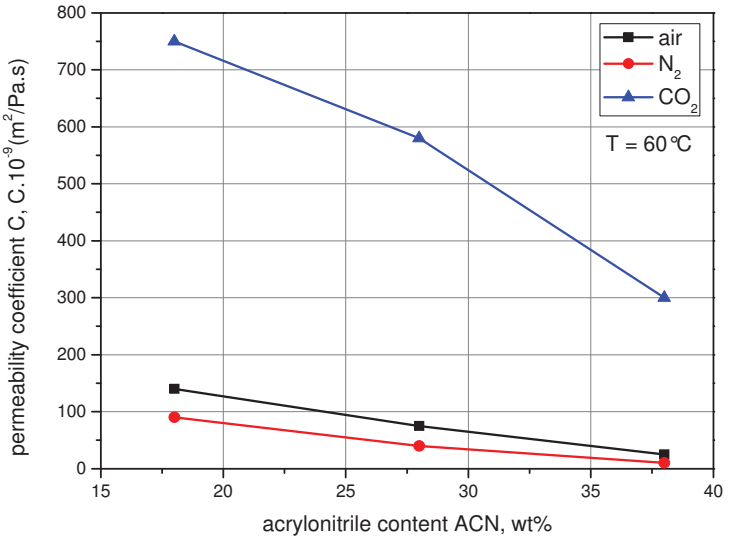

Figure 2.2: Permeability coefficient in dependence of the acrylonitrile content for air, N_2 and CO_2 [Sommer and Röthemeyer, 2006]

For the application as sealing material, the compression set and the oil durability are very important. In general, the compression set shows an opposite behavior to the oil durability. Because of the relatively high glass transition temperature, the gas permeability is comparatively small, as shown in Figure 2.2. Furthermore, as mentioned before, the gas proofness is also a function of the ACN content. Blends with NBR and Poly Vinyl Chloride (PVC) are possible to improve the gas permeability and strength, but the elasticity, the compression set and mainly the flexibility at low temperatures decrease [Sommer and Röthemeyer, 2006].

2.1.2 Hydrogenated nitrile butadiene rubber (H-NBR)

H-NBR is manufactured by means of catalytic hydrogenation of Nitrile Butadien Rubber. A controlled process is necessary to reduce just the double bond and not the nitrile group. Complete hydrogenated rubber shows heat stability up to 155°C [Nagdi, 1993, Schmitt, 1987]. As depicted in Figure 2.1, the glass transition temperature is mainly influenced by the ACN content. In general, the increment of the slope for H-NBR is less than for NBR.
The lack of double bond makes this rubber having higher heat-/weathering-/ozone and oil resistance in comparison to NBR. Filled systems typically have a hardness of 40 to 90 Shore A and tear strength up to 45MPa. Similar fillers as for NBR are used for H-NBR. Middle active carbon blacks, like N550 and N762, improve the mechanical properties. High active carbon black is reflected in the high value of the viscosity. Non-black fillers are used to intensify the aging resistance. To increase the filler/polymer interaction, silane is required [Sommer and Röthemeyer, 2006].

Two different groups of fillers, activate and inactivate ones, can be used. Activated fillers change the viscoelastic properties, furthermore an enhanced viscosity and better fracture behavior are reached. Inactivated fillers are used to improve the processability and gas permeability. These fillers weaken the matrix and decrease the fracture energy of the vulcanised rubber.

3 basic properties to describe the cumulative influence of the filler have to be considered [Sommer and Röthemeyer, 2006]:

- contact surface (extensity factor)
- surface activity (intensity factor)
- structure (geometric factor)

The reinforcement, which is reached by the filler, depends on the contact surface of the rubber. Assuming nonporous filler in the matrix, the contact surface per unit of volume is defined by equation I:

$$A = \varphi \cdot \rho \cdot S \quad \text{(I)}$$

φ … volume fraction of the filler, [-]

ρ … density of the filler, [kg/cm³]

S … specific surface area, [m²/kg]

The surface activity describes the interaction between filler and rubber. This parameter is influenced by functional groups and free radicals near the surface. Polymer molecules are linked to the surface using physical or chemical adsorption or covalent connections. Due to the adsorption, a rubber shell formation called bounded rubber occurs. To assign the bounded rubber part extraction a dissolver is used. The part of rubber which is attached to the surface with a very good dissolver is called the bounded rubber.

The filler morphology can be described by structure including size, aspect ratio and size distribution. Primary particles are the smallest homogenous units specified by the microstructure. Through clustering, the smallest stable structure called aggregate is refined. Multiple aggregates, under the influence of van der Waals forces, can stick together generating a secondary structure. In contrast to the aggregates, this secondary structure can be destroyed through the mixing process.

Stiffness increase by fillers

Analytical models and micromechanical modelling describe the stiffness increase by fillers. The analytical part is discussed by Smallwood [Smallwood, 1944] for small deformations, small concentrations and spherical particles. With rising concentration of the filler particle Guth and Gold relationships were used [Sommer and Röthemeyer, 2006]. Due to the possibility of saving a lot of money for test series and and model materials, the micromechanical modelling part is getting more and more important for the industry. Based on the results of mechanical investigations, material models were assumed [Dommelen et al., 2004, Jerabek, 2008, Gastl, in Prog.].

Fracture behavior

Basically, two path ways of vulcanised rubber fracture can occur. Imperfections (like inhomogeneity, impurity, micro pores and local network defects) or surface defects (like ozone tear, cuts) cause failure of the material. Inhomogeneities and micro pores with a diameter larger than 100nm may reach the critical crack propagation energy resulting in a significant crack growth. The critical stress initiating crack propagation is dependent on the vulcanised rubber-filler interaction and, as mentioned before, on the surface area. As depicted in Figure 2.3, the stress for crack initiation rises with the increasing surface and surface activity.

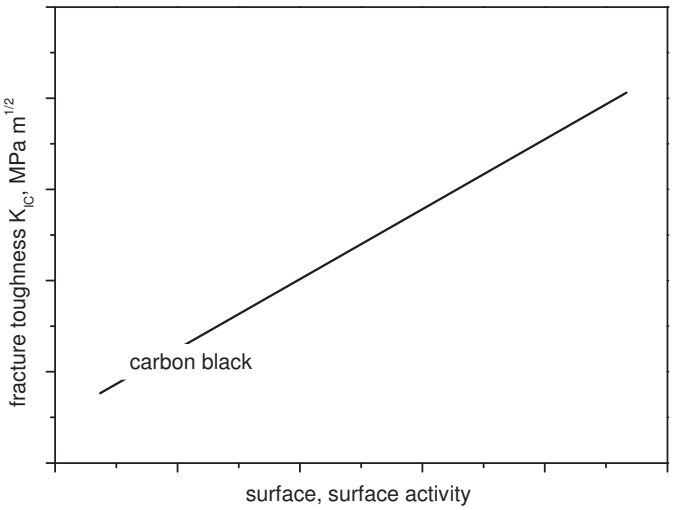

Figure 2.3: Influence of the filler surface/surface activity on the critical stress for crack initiation [Sommer and Röthemeyer, 2006]

The increasing ACN content shows a similar behavior to the dependence of the surface and surface activity. With this increment, the stress for crack initiation also augments to higher values. Carbon black tends to clustering of the aggregates with increasing surface, which causes inhomogeneities.

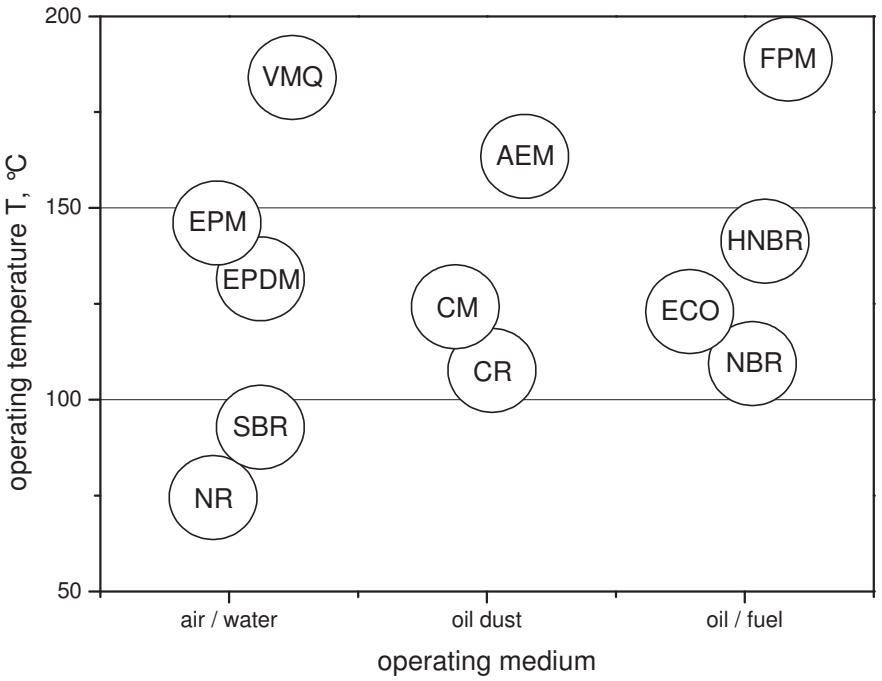

Figure 2.4: Temperature resistance of different rubbers

Rising application temperatures for specific applications, require special rubber materials. Figure 2.4 shows the temperature resistance of different rubbers for different operating mediums. As depicted, HNBR is one of the best materials to be used up to 150°C. Furthermore, HNBR shows a good resistance against oil and fuel.

2.2 Rapid gas decompression behavior

Oilfield seals and hoses are exposed to high temperatures, aggressive fluids and variations of gases. High pressure and different gases can induce an error called the rapid gas decompression failure. This failure appears as crack growth, extensive deformation, swelling, blisters and in some cases catastrophic fragmentation of the vulcanised rubber. The failure process can be basically divided into 2 phases, the pressurization or compression part and the depressurization or decompression part.

2.2.1 Compression phase

In the first phase, the pressurization, the seal is exposed to high temperatures and high pressure gases. These ambient conditions result in a volume change of the material because of the saturation of the material with supercritical gas. This volume increase is visible to the naked eye and depends strongly on the temperature, the pressure and the gas.

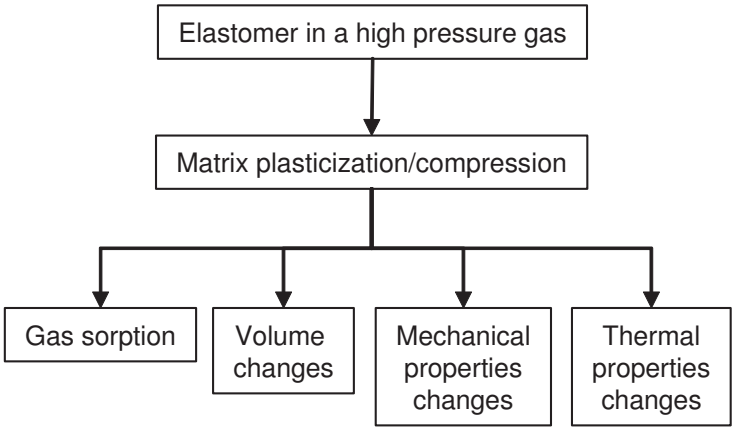

Figure 2.5: Overview of the effects occuring during pressurization [Briscoe et al., 1994]

As depicted in Figure 2.5, the mechanical and thermal properties are also modified by the amount of solved gas. Hence, a new material with completely different properties is obtained [Stevenson and Morgan, 1995]. The volume change and the change of the properties converge to an equilibrium value, which is dependent on temperature, pressure, gas and the material composition. If the material is saturated, the properties and the volume are constant.

2.2.2 Decompression phase

The depressurization part is a highly complex part resulting in a significant volume increase up to 500% because of the rapid pressure drop. The release of the pressure causes blisters and voids in the material. For the description of this process, 4 basic ideas are essential [Briscoe et al., 1994]:

- the gas modifies the mechanical and thermal properties of the material.
- with the removal of the pneumatic stress a triaxial tensile stress appears.
- a thermal profile is produced during adiabatic cooling.
- gas concentration profile is build up within the material.

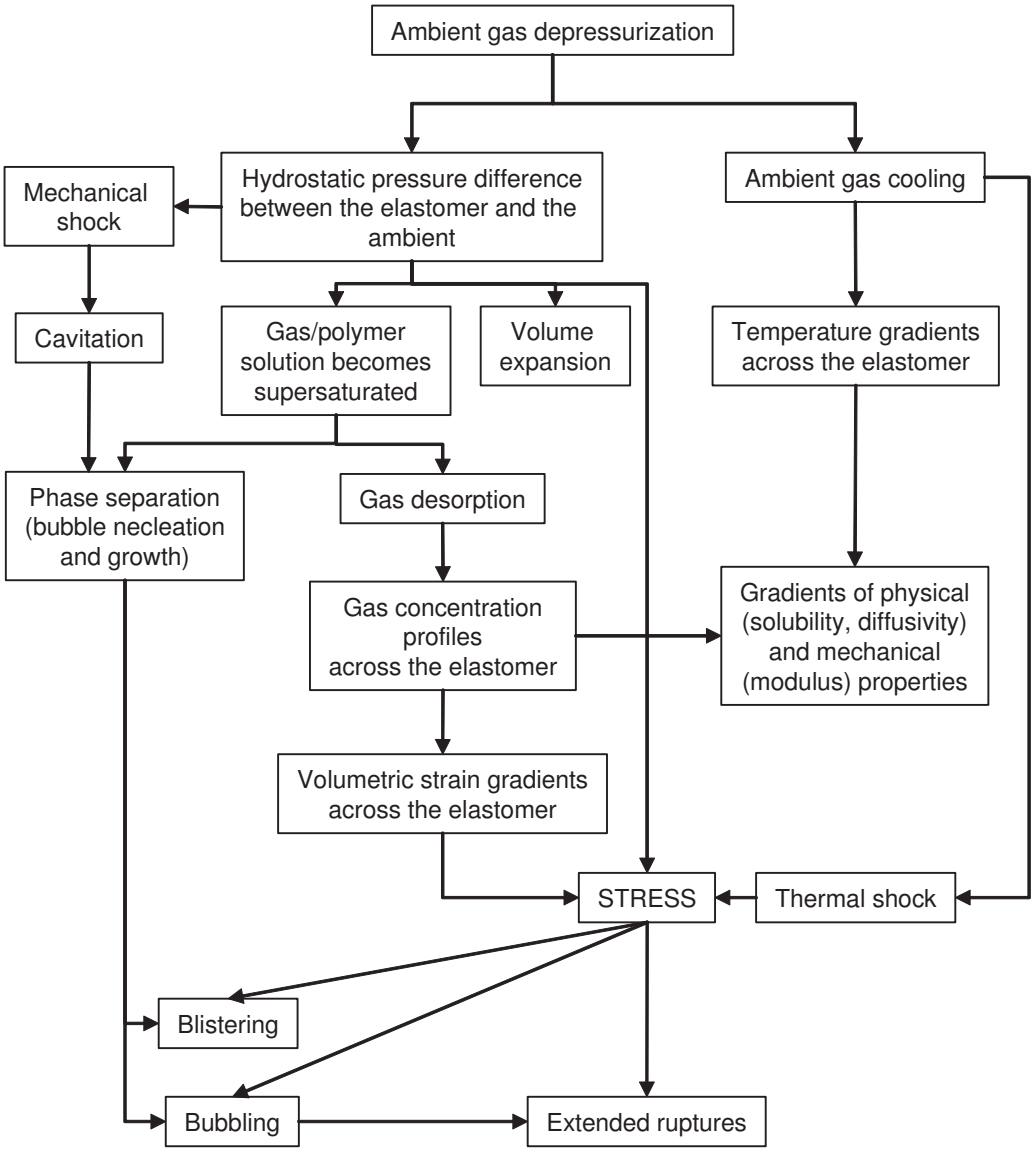

Figure 2.6: Overview of the effects occuring during depressurization [Briscoe et al., 1994]

The interactions of the different phenomena resulting in stress induced failure are depicted in Figure 2.6. At the start of depressurization, two main effects happen. First off all, ambient gas is cooling which results in a temperature gradient across the material and a thermal shock. Because of the temperature dependent properties of vulcanised rubber, a mechanical and physical properties profile across the material is produced. The second effect is the hydrostatic pressure difference between the vulcanised rubber and the ambience. The pressure difference results in 4 main effects: a mechanical shock, a supersaturated gas/polymer solution, a volume expansion and stress. The mechanical shock causes cavitations followed by bubble nucleation and growth, resulting in blistering

and bubbles in the material. Furthermore, a gas concentration profile across the vulcanised rubber is produced because of the supersaturated gas/polymer solution. Anyway, all effects result in stress of the material which causes blistering, bubbling and extended ruptures.

2.3 Physical processes during compression and decompression phase

Briscoe described two distinct phenomena for vulcanised rubber exposed to various gas compositions [Briscoe et al., 1994]. The first phenomenon is the dissolution of gas in the polymer matrix which causes a plasticization of the material. Additionally, the mobility of the polymer chains and the free volume increase. The second phenomenon shows the opposite influence on the mobility of the polymer chains and the free volume because of a matrix compression due to the applied pressure. However, the resulting polymer gas solution creates unique thermal and mechanical properties.

The state produced during the pressurization process is disturbed by the depressurization process. Due to the reduction of the pressure, the release of the compressive strain of the material (stored during pressurization process) results in an expanding polymer. Additionally, the elastomer becomes supersaturated and bubbles (out of the solution) occur. Furthermore, desorption processes occur, creating a step concentration profile along the cross section of the vulcanised rubber.

Conditionally to these phenomena, crack initiation and propagation occur. To describe this process, knowledge on the gas solubility at high pressure is needed to predict the concentration of gas across the elastomer. Moreover, also the mass sorption is of importance, to provide information on the developed gas transport and the concentration profiles. Further, also the volume change at equilibrium is of interest, to give information on the gas induced plasticization value.

2.3.1 Gas induced changes of the material

The matrix plasticization initiated by the dissolve process of the gas is not directly related to the rapid gas decompression failure, but important for the description of the induced plasticization, the mechanical properties and the degree of super saturation. Information about the solubility and the diffusion of gases in polymer

materials is given by Amerongen [Amerongen, 1964] and Crank [Crank and Park, 1968]. For low gas pressures, Henry's law can be used

$$c = S \cdot P \tag{II}$$

where c stands for the concentration of permanent gas in the elastomer. S is the solubility coefficient of the gas in the elastomer and P the ambient pressure. To discuss higher pressures, a derivation of Henry's law is necessary. Liatsis [Liatsis, 1989] use such derivations to describe the sorption of CO_2 in a nitrile rubber. Furthermore, Fleming and Koros [Fleming and Koros, 1986] showed an adequate statement by using the Flory-Huggins equation for CO_2 and silicon rubber for pressures up to 6 MPa:

$$ln\left(\frac{P}{P_0}\right) = ln\left(1-\nu_p\right) + \nu_p + \chi \cdot \nu_p{}^2 + \frac{V_1 \cdot \nu_e}{V_0} \cdot \left(\sqrt[3]{\nu_p} - \frac{\nu_p}{2}\right) \tag{III}$$

P … ambient pressure

P_0 … vapour pressure of the penetrant

ν_p … volume fraction of the polymer

χ … Flory Huggins interaction parameter

V_1 … molar volume of the penetrant

ν_e … effective number of crosslinks expressed in moles

V_0 … volume of the dry polymer

Basically, the solubility increases with the critical temperature or the boiling point of the gas [Amerongen, 1964, Shah et al., 1986, Stern et al., 1969]. This experimental observed correlation can also be discussed in thermodynamic considerations [Gee, 1947, Stern and Shiah, 1981]. Furthermore, the polymer structure, especially the side groups attached to the polymer chain, affect the solubility of the vulcanised rubber. These side groups influence the free volume of the material and the interaction between the molecular chain and the gas molecules. Bulkier side groups increase the solubility and with ascending acrylonitrile content the solubility raises.

Moreover, the effect of gas sorption is highly dependent on the filler/matrix interface. As discussed in literature, the gas sorption decreases for stronger filler/matrix interfaces [Melikhova et al., 1959, Carpenter and Twiss, 1940]

because of the higher adsorption of the polymer in regions near the filler surface. By this effect, a higher modulus near the filler particle is reached and thus the gas sorption of the vulcanised rubber is reduced. For a weaker filler/matrix interface the gas sorption and the probability of a filler/matrix stripping increases. Based on this debonding, the chance of forming voids and cavities filled with high pressure gas escalates. Additionally, the solubility decreases with rising temperature. This temperature dependence is expressed by the Van't Hoff relationship in the regime of pressure where Henry's law is valid [Shah et al., 1986, Kamiya et al., 1986].

$$S = S_0 \cdot e^{-\frac{\Delta H_s}{R \cdot T}} \qquad \text{(IV)}$$

S … solubility coefficient of the gas in the polymer

S_0 … constant

ΔH_s … heat of the solution

For polymers exposed to high pressure, the swelling is often connected to mass sorption, as discussed in literature by Griffiths [Griffiths, 1985], Fleming [Fleming and Koros, 1986]. A volume increase of about 20-30% improves the sealing ability, but exceeding volume change is unrequested [Ender, 1986]. This volume dilatation is directly related to the mechanical properties of the material. Especially for elastomers, the volume change depends on the swelling potential of the gas, the gas pressure and the polymer system [Ender, 1986]. Gases with high solubility in polymers, like CO_2, SO_2, H_2S, act as strong swelling agents. However, also the filler/matrix interface strongly influences the volume change of the polymer. Generally, a lower change is observed for filled elastomers than for unfilled ones [Briscoe and Zakaria, 1992].

The problem of the rapid gas decompression failure is related to the diffusion of absorbed gas in the vulcanised rubber. As mentioned before, the absorbed gas produces a concentration profile across the elastomer. This profile is closely associated with the stress fields which induce mechanical failure. Thus, the mechanical properties of the vulcanised rubber are a function of the absorbed gas. Regrettably, studies of diffusion at similar ambient conditions are rare.

Generally the diffusion is divided into three different categories, case I the Fickian case, case II and case III the non-Fickian case. Fick's first law is used to describe the Fickian diffusion in case I [Crank, 1975],

$$J = -D(u) \cdot \nabla u \tag{V}$$

where J is the concentration flux vector and u the concentration. Further, $D(u)$ is the classical diffusion coefficient. For case II the penetration of diffusing substance is much faster than any relaxation process of the matrix material. Case III is characterized by observed curves which cannot be described with Fick's law [Crank, 1975]. To explain the concentration behavior in diffusion processes in polymers the classical Fick's law should be replaced by another relation/equation [Vorotnikov, 2009] which was proposed by Cohen [Cohen at el., 1991 and 1995] for the diffusion of a penetrant liquid in a polymer, based on the relaxation mechanism:

$$J = -D(u) \cdot \nabla u - E(u) \int_{-\infty}^{t} exp\left(\int_{t}^{s} \beta(u(\xi, \chi) d\xi \right) f\left(u(s, \chi), \frac{\partial u(s, \chi)}{\partial s} \right) ds \tag{VI}$$

scalar function β … inverse of the relaxation time.

scalars D, E … diffusion and stress diffusion coefficient.

function f … represents the dependence of the relaxation on the concentration field and its rate of change.

The additional integral describes the non-Fickian constituent of the concentration flux which depends on the local concentration history of the process.

However, in general the diffusion can be approximated by Fick's law because of the higher chain mobility at ambient temperature (above glass transition temperature) [Fujita, 1968]. For low pressures, the diffusion coefficient is independent of the concentration of the penetrant, but for increasing pressure the diffusivity becomes concentration-dependent [Amerongen, 1964]. Further, an increase of the diffusion coefficient is observed for permanent gases, as CO_2, because the gas dissolves significantly in the rubber resulting in a plasticized matrix which causes a rising diffusion coefficient. The matrix compression by the ambient gas should be considered as additional factor, inducing reduction of the free volume resulting in a decreased diffusivity. Both described cases of increasing

the diffusion coefficient by permanent gas and of decreasing the diffusion coefficient by the matrix compression strongly depend on the concentration of the penetrant and the pressure. Permeation studies by Campion [Campion, 1990] and Jordan [Jordan and Koros, 1990] and pure diffusion studies by Briscoe [Briscoe et al., 1992] dispute this concentration and pressure dependent behavior.
Furthermore, literature describes the temperature effect with the well known Arrhenius relationship as depicted in equation (VII) [Amerongen, 1964, Stern et al., 1987]. In general, the diffusion coefficient of the vulcanised rubber increases with rising temperature

$$D = D_0 \cdot e^{-\frac{E_d}{R \cdot T}} \qquad \text{(VII)}$$

E_d … energy of activation

D_0 … pre-exponential factor

To avoid rapid gas decompression failure, knowledge on the interrelationship of diffusion processes is required. Unfortunately, existing studies describe this interrelationship at low pressures [Amerongen, 1964, Stern et al., 1987]. The diffusion process is basically described by the movement of the penetrant molecules through micro cavities. These micro cavities are permanently created and destroyed by the Brownian motion of segments of the polymer chain [Amerongen, 1964]. Larger molecules require larger cavities to penetrate. Thus, the activation energy for diffusion is much higher resulting in a lower diffusivity. Furthermore, bulky functional groups (e.g. vinyl or methyl) in the side or main chain of the polymer decrease the diffusivity, due to the decrease of the chain flexibility.

Finally, the cross linking density and the used filler particles also affect the diffusivity of the vulcanised rubber. Usually, the mechanical properties are modified by controlling the cross link density or by adding filler particles. When the chemical cross linking raises, the segmental mobility of the polymer chain decreases, resulting in a reduction of the gas diffusivity. Additionally, fillers also reduce the diffusivity of gases in elastomers, when they are impermeable by the gas, increasing the effective diffusion length through the vulcanised rubber

[Amerongen, 1964]. Hence, lamellar fillers have a more pronounced effect on the diffusion. The orientation of the filler influences the diffusivity, especially for elastomers used as a membrane. Furthermore, a decrease of the diffusivity around filler particles due to the reduction of the chain flexibility is observed [Tanioka et al., 1982].

Most important in the sense of influencing the mechanical properties of the vulcanised rubber is the plasticization or the compressive impact of the penetrant. By using a pressurizing medium such as N2, the free volume is being decreased because of the decrease of the molecular motion. In contrast, plasticization penetrative medium cause an increase of the free volume due to the increasing molecular motion. This increase or decrease has an impact on the glass transition temperature of the material and as a consequence, the mechanical properties change [Briscoe et al., 1994].

2.3.2 Failure

During the pressurization process an amount of elastic strain is stored in the vulcanised rubber. Due to the pressure difference between the interior and the ambience during the depressurization process this stored strain is released and the elastomer expands. Concerning the negative hydrostatic pressure, cavities are initiated and grow in the material. These cavities start to expand in an unstable manner when a critical pressure difference between the interior and the ambience is reached. Briscoe and Zakaria [Briscoe and Zakaria, 1990] announced the volumetric change during decompression of silicon elastomer exposed to high pressure N_2.

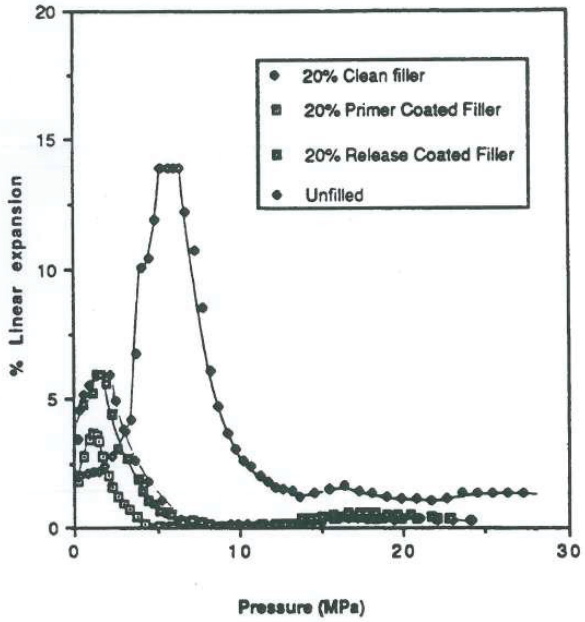

Figure 2.7: Percentage of linear inflation for various silicone elastomer specimens as a function of ambient pressure during depressurization in an N_2 atmosphere [Briscoe et al., 1994]

As depicted in Figure 2.7**,** a small initial expansion followed by a large expansion is observed. The first volumetric change is linked to the appearance of cavities. In the second step the cavities start to expand by casing crack formation and crack propagation. For elastomers exposed to high pressure CO_2 sharp spikes are observed attributed to the rupture and collapse of large bubbles. Zakaria noticed a lower maximum expansion for filled elastomers than for unfilled vulcanised rubber [Zakaria, 1990].

Due to the adiabatic nature of the rapid gas decompression process, the temperature effect should be considered. Gases with a higher Joul-Thompson effect cause a larger temperature decrease, thus the temperature effect is more pronounced for CO_2 than for N_2. This temperature difference between the elastomer and the gas causes a heat transfer, producing a temperature profile across the vulcanised rubber. Due to the temperature dependence of the mechanical properties a mechanical properties gradient is developed across the elastomer.

The key to design stress fields during depressurization is to understand the fracture and the propagation of failures. As mentioned before, the vulcanised rubber absorbs the ambient gas until the equilibrium is reached. This balance is disturbed during the depressurization process when the ambient pressure is

released. Due to the gas release, a concentration and fugacity profile is produced at the cross section of the polymer. Similar to the temperature gradient, the volumetric strain is not uniform across the vulcanised rubber, but decreases from the interior to the surface.

Elastomers under uniform triaxial tension are well documented in literature [Gent, 1990]. Gent and Lindley [Gent and Lindley, 1958] observed a number of small cracks uniformly distributed across the vulcanised rubber samples. Later, Lindsey depicted that failure initiation occurs when voids appear and expand in a spherically radial fashion [Lindsey, 1967]. Similar phenomena during depressurization were announced by Gent and Tompkins [Gent and Tompkins, 1969]. Further they proposed that a number of blisters preexist in the form of sub microscopic voids across the material. These voids are produced during the processing of the elastomer when air is trapped during manufacturing or the particles are badly wetted. During the pressurization process, the voids get filled with high pressure gas and expand during the depressurization process due to the pressure difference. Further, these cavities expand during the exposure of gas and then collapse when the gas is depleted. When the cavity attains the maximum elasticity of the material, a crack is formed and propagates by a tearing process [Lindsey, 1967].

In filled elastomers, a more complex process concerning the two failure modes is observed. The first mode, cohesive failure, appears in the polymer matrix because of the triaxial tension. The second mode, interfacial failure, describes the separation of the polymer from the filler surface [Gent and Park, 1984, Gent, 1984].

To give a failure criterion, Gent and Tompkins model a simple void with the radius r_0, which expands indefinitely in a block with infinite dimensions [Gent and Tompkins, 1969]. The pressure difference ΔP needed to expand the void ($r>r_0$) is determined by the theory of rubber-like-elasticity:

$$\Delta P = \frac{G}{2} \cdot \left[5 - 4 \cdot \left(\frac{r_0}{r} \right) - \left(\frac{r_0}{r} \right)^4 \right] + 2 \cdot \frac{\gamma}{r} \qquad \text{(VIII)}$$

where G is the shear modulus, γ the surface energy, r the radius of the void and r_0 the initial radius. For voids with a large initial radius (r_0>10-5 cm) the term of surface energy can be disregarded:

$$\Delta P = \frac{G}{2} \cdot \left[5 - 4 \cdot \left(\frac{r_0}{r} \right) - \left(\frac{r_0}{r} \right)^4 \right] \tag{IX}$$

For an infinite expansion ($r \to \infty$), the critical pressure difference is defined by:

$$\Delta P_c = 5 \cdot \frac{G}{2} = 5 \cdot \frac{E}{6} \tag{X}$$

According to equation (X) [Derham and Thomson, 2003], the critical pressure difference is independent from the initial radius and just a function of the young's modulus. A different approach for the cavity expansion is given by fracture mechanics. Griffith's energy criterion describes a spherical volume V_0 which grows when the value of the elastic energy exceeds the characteristic fracture energy G_c.

$$-\left[\frac{\partial \left(W_{el} + W_p \right)}{\partial A} \right] \geq G_c \tag{XI}$$

$$W_p = P \cdot dV \tag{XII}$$

$$W_{el} = \int_{V_0}^{V} P \cdot dV \tag{XIII}$$

where W_{el} is the elastic energy stored in the matrix, W_p the work performed by the pressure and A the surface area of the cavity. Williams [Williams and Schapery, 1965] and Gent [Gent and Wang, 1991] observed a strong dependence on the initial radius by applying this approach. Hou and Abeyaratne discuss the problem of the unbounded elastic expansion of a spherical cavity under non-symmetric loading [Hou and Abeyaratne, 1992]. If the principal stress applied on a neo-Hooken medium is denoted by σ_1, σ_2 and σ_3 then

$$\left(4 \cdot \sigma_1 - \sigma_2 - \sigma_3\right) \cdot \left(4 \cdot \sigma_2 - \sigma_3 - \sigma_1\right) \cdot \left(4 \cdot \sigma_3 - \sigma_1 - \sigma_2\right) \geq \frac{125 \cdot E^3}{27} \tag{XIV}$$

For the case of pure hydrostatic tension, where $\sigma_1 = \sigma_2 = \sigma_3 = P$, equation (XIV) is reduced to equation (X).

As mentioned before, the failure propagation starts when a critical strain level at the void wall is reached due to the elastic expansion. This threshold tearing energy

is of the order of 0,1 kJ/m^2. A general form of experimental measurements is depicted in Figure 2.8. A time dependent crack growth is observed in the range of low tearing energy [Kadir and Thomas, 1979, Lake et al., 1991]. For medium tearing energy stick slip behavior occurs with a fluctuating crack growth rate. Constant propagation resulting in a catastrophic failure is observed for high tearing energy.

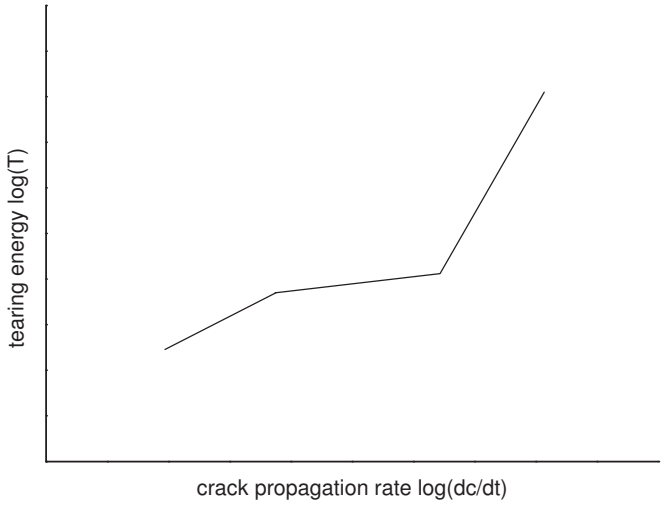

Figure 2.8: Increase of tearing energy with increasing crack growth rate

This behavior is mainly illustrated for non-crystallizing elastomers and associated with the ability of rubber to dissipate tearing energy. The maximum propagation velocity is independent of the available energy for tearing and is just one function of the stored elastic strain in the vulcanised rubber exposed to high pressure. The addition of filler particles increases the tearing energy whereas a rising temperature results in a decrease of the tearing energy.

Due to the negative hydrostatic pressure and the gas desorption from the surrounding polymer matrix during the depressurization process microscopic voids form visible cavities. Gent [Gent and Tompkins, 1969] and Stewart [Stewart, 1970] observed experimentally and theoretically, that the bubble growth rate is proportional to the square root of the elapsed time after nucleation, where k is a constant which increases with rising diffusivity and solubility.

$$r = k \cdot \sqrt{t} \qquad \text{(XV)}$$

For the visible estimation of the area of fracture a rough surface with a surrounded glass-like surface is observed. This indicates a slow crack growth rate until a defined size is reached, resulting in a catastrophic failure. Briscoe and Zakaria [Briscoe and Zakaria, 1990] show a strong effect of the filler particles and the quality of the filler/matrix interface for filled elastomers. A higher mean length of crack is observed for unfilled samples, but in filled materials a higher number of cracks occur. During the decompression process, the gas interface expands forming small bubbles and decreasing the filler/matrix bound until the failure is reached, where the filler/matrix interface act like a 'zip'. Based on Figure 2.8 the velocity of crack propagation is described by:

$$\frac{dc}{dt} = B \cdot T^n \tag{XVI}$$

where B and n are constant, depending on the linear section. Andrews and Stevenson show a relation of the young's modulus E and the tearing energy T for a penny shaped crack [Andrews and Stevenson, 1978].

$$T = \frac{P_c^{\,2} \cdot \left(1-\nu^2\right) \cdot c}{E} \cdot \left[\frac{3}{32} \cdot \left[\left(\frac{c}{h}\right)^3 + \frac{c}{h} \cdot \frac{4}{\left(1-\nu\right)}\right] + \frac{1}{\pi}\right] \tag{XVII}$$

where c is the radius of the crack, h is half of the thickness of the sheet and ν the poisson's ratio. Equation (XVII) indicates, that an increase of the young's modulus results in a decrease of the tearing energy and the crack propagation rate. As mentioned before, CO_2 induces a matrix plasticization causing a reduction of the young's modulus. Therefore the tearing energy and the possibility of catastrophic failure are higher.

2.4 Standard test method

2.4.1 NACE, TM0192-2003

The NACE standard, "Effects of High-Temperature, High-Pressure Carbon Dioxide Decompression on Elastomeric Materials", describes a test method to measure the effect of rapid gas decompression failure on vulcanised rubber seals exposed to CO2. No pass/fail criteria are provided for tested materials. By means of this test method, the rapid gas decompression resistance of elastomers under specific conditions can be qualitatively measured. For the evaluation, O-rings with an

internal diameter of 37,47mm and a cross section of 5,3mm should be used. The vessel volume should be 25 times greater than the total specimen volume. Possible test temperature and test pressure are listed in Table 2.2. The exposure period should be a minimum of 24 hours +-1hour.

Table 2.2: Test temperature and test pressure for the NACE standard test method

Test temperature	Test pressure
50, 100, 120, 150, 175 or 230 +-3°C	7, 17, 28, or 38 +-0.7MPa

Nine specimens for one complete test series are required. Three of the test specimens are used to determine the hardness, cross sectional diameter and the tensile properties. The other six specimens are exposed to temperature and pressure in the vessel. The vessel should be charged with a minimum rate of 0.7MPa/minute. The depressurization rate is fixed to a constant rate of 7 +-0.7MPa. After the decompression, the changes of visual appearance, in tensile properties and of cross-sectional diameter should be documented. For the determination of external and internal damage, three of the six exposed specimens are used, see Table 2.3. The other three specimens are needed to determine the tensile properties.

Regarding the NACE standard test method, the following aspects should be considered:

- date and temperature of testing room,
- material parameters,
- test environment,
- test temperature,
- test pressure,
- test exposure period,
- decompression time and rate,
- number of depressurization cycles,
- recorded elapsed time from depressurization to tensile testing,
- calculated properties for applicable properties (cross sectional diameter, durometer hardness and tensile properties),

$$\%\,change\ of\ exposed\ specimen = \left(\frac{value\ exposed - value\ original}{value\ original} \right) \cdot 100$$

- information on the physical condition of the exposed specimens,
- other pertinent observed and recorded data,
- information on whether specimens were tested in a free or constrained state.

Table 2.3: Rating of the material for the NACE standard test method

Rating	Description of Damage
1	No visible damage
2	Minimal damage confined to the surface (few blisters and cracks)
3	External and internal damage (many blisters and cracks
4	Extensive damage, fragmentation

2.4.2 NORSOK, M710-2001

In contrast to the NACE standard test method, the NORSOK standard comprised additional requirements for the qualification of manufacturers, the qualification of elastomeric sealing materials and qualification of thermoplastic materials including ageing tests. Test media, conditions, equipment and procedures for rapid gas decompression testing of elastomeric materials is described in annex B. Different constrained measurements can be implemented, as depicted in Figure 2.9.

Figure 2.9: Constrained test set-up for two specimens

Furthermore, the acceptance criterion for the seal cross section is not to have a rating of higher than three. For this test method, different media mixtures are defined in Table 2.4.

Table 2.4: Used gas mixtures for different applications defined by NORSOK standard

Sweet/Sour Wells/ low CO_2	**Sweet/Sour Wells/ high CO_2**	**CO_2 injection Wells**
3% CO_2, 97% CH_4	10% CO_2, 90% CH_4	100% CO_2

The test temperature should be one of the following temperatures: 100, 150 or 200°C. Before applying the gas pressure, the test specimen should be kept at test temperature for at least 10 minutes. The test pressure should be fixed at 15, 20 or 30 MPa. As standard test specimen, an O-ring seal of an internal diameter of 37,47mm and a cross section of 5,33mm is used. For an objective result, a minimum of three O-rings should be tested. The test is carried out at constrained conditions whereby the O-ring is compressed by 20%. The standard initial exposure period should be 72 hours. After this exposure period, the decompression rate should be fixed at 2-4MPa/minute. A second pressurization cycle (holding time 23 hours) is applied after a holding period of 1 hour at ambient pressure. This pressure cycling should be continued for 10 cycles. For the visual appearance of the seals the seals are cut into 4 equal radial sections as shown in Figure 2.10.

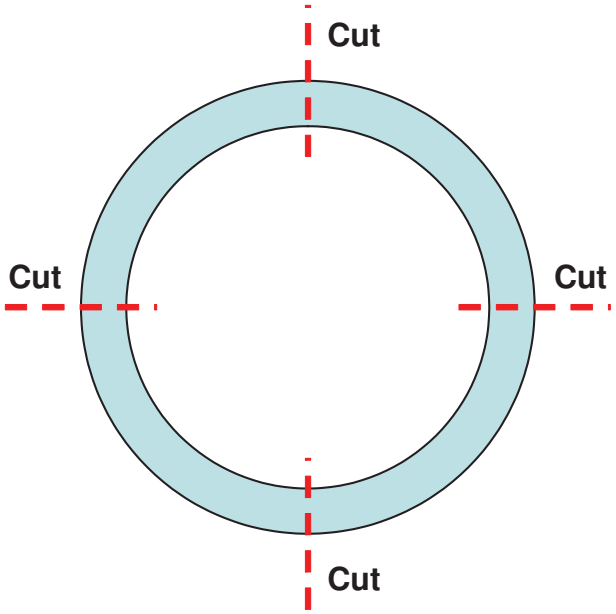

Figure 2.10: Preparation of pressurized O-ring seals for visual rating

For the visual rating a magnification of at least 10 times is necessary. In Table 2.5 a rating for the cross section between 0 and 5 is provided. As mentioned before, seals with a rating higher than 3 are not acceptable.

Table 2.5: Rating for the visual inspection defined by NORSOK standard

Description	Rating
No internal cracks, holes or blisters of any size.	0
Less than 4 internal cracks, each shorter than 50% of cross section with a total crack length less than the cross section.	1
Less than 6 internal cracks, each shorter than 50% of the cross section with a total crack length of less than 2,5 times the cross section.	2
Less than 9 internal cracks of which max. 2 cracks can have a length between 50% and 80% of the cross section.	3
More than 8 internal cracks or one or more cracks longer than 80% of the cross section.	4
Crack(s) going through cross section or complete separation of the seal into fragments.	5

The test report regarding to the NORSOK standard should include information on:

- date of test,
- seal reference information,

- composition of test medium,
- initial observations,
- temperature records,
- test pressure records,
- rapid gas decompression damage by a rating system,
- any other pertinent observations or records.

2.4.3 Comparison of NACE and NORSOK

Both engineering standards are compared regarding their test procedures in Table 2.6 As depicted the NACE standard shows a higher variation of the test temperature and the test pressure than the NORSOK standard. The NACE standard deals with a higher number of specimens than the NORSOK and describes further investigations. Moreover NACE shows a shorter testing time and a higher decompression rate in direct comparison.

Table 2.6: Comparison of the test conditions for NACE and NORSOK

Test procedure	NACE	NORSOK
test temperature	50,100,120,150, 175 or 230℃	100, 150 or 200℃
test pressure	7, 17, 28 or 38 MPa	15, 20 or 30 MPa
test specimen	internal diameter: 37.47mm cross section: 5.33mm	internal diameter: 37.47mm cross section: 5.33mm
gases	CO_2	CO_2, CH_4
number of specimens	min. 9	min. 3
testing condition	free and constrained	constrained
testing time	min. 24 hours Single	72 hours initial 23 hours afterwards multicycle
decompression rate	7MPa/min	2-4MPa/min

Table 2.7: Comparison of the evaluation for NACE and NORSOK

Test standard	Number of specimens	Evaluation	Rating
NACE	9	internal and external damage, further investigations e.g. tensile properties, hardness.	**1 – 4** no pass/fail criteria
NORSOK	3	internal and external damage.	**0 – 5** higher than 3 not acceptable

Table 2.7 shows the different evaluation criteria and the rating for both standards. In addition to the investigation of the internal and external damage, further measurements are described by the NACE standard. In contrast to the NACE standard, the NORSOK standard provides clear acceptance criteria for tested materials. Figure 2.11 gives a short overview of 4 tested materials and the NORSOK ranking. The testing conditions are depicted in Table 2.8. The ranking of the material is based on the size and the frequency of the observed cracks.

Table 2.8: Used test parameters for test with NORSOK standard

Test procedure	NORSOK
test temperature	150℃
test pressure	15MPa
gases	10% CO_2 and 90% CH_4
decompression rate	2MPa/min
cycle	10

HNBR

NORSOK: **4**

multiple cracks

HNBR1

NORSOK: **1**

single crack

HNBR2

NORSOK: **3**

multiple cracks

HNBR3

NORSOK: **0**

no cracks

Figure 2.11: Examples for tested materials

3 EXPERIMENT

3.1 Materials

As discussed in the literature part of this thesis, hydrogenated nitrile butadiene rubber seems to be the best material for these special applications and the ambient conditions. Overall, 4 experimental materials were used, provided by SKF Economos GmbH. The first material is a hydrogenated nitrile butadiene rubber filled with carbon black. In the following discussions this material will be called HNBR. HNBR1, the pseudonym for the second material, is filled with the same carbon black as HNBR including an additional filler component, filler 1. The third material HNBR2, which is used for the test series, contains the same amount of carbon black and filler 1 as HNBR1. Only the acrylonitrile content is modified to higher values. For the fourth material HNBR3, the acrylonitrile content and the filler system is varied. Table 3.1 combines the used materials showing the different used formulation.

Table 3.1: Overview of the used materials

Pseudonym	Formulation
HNBR	H-NBR Filled with carbon black
HNBR1	H-NBR Filled with carbon black + filler 1
HNBR2	H-NBR filled with carbon black + filler 1 Increase of the ACN content
HNBR3	H-NBR filled with carbon black + filler 2 further increase of the ACN content

3.2 Material characterization

As mentioned in chapter 2, one of the important steps to understand the rapid gas decompression process, is the knowledge of the properties of vulcanised rubbers.

Thus, the thermal as the mechanical characterization is of particular interest. The dynamic mechanical characterization and the characterization with compression tests will be described in this thesis.

3.2.1 Dynamic mechanical analyses

Tensile loaded dynamic mechanical measurements were used for the evaluation of the storage modulus at testing temperature and to observe the influence of the varying acrylonitrile content.

3.2.1.1 Test equipment

Dynamic mechanical analysis (DMA) tests were performed using the novel electro-dynamical testing machine, GABO Eplexor 100 N [Ahlden, Germany]. In Figure 3.1 the used tensile test set-up is depicted.

Figure 3.1: Test set-up for dynamic mechanical measurements

3.2.1.2 Specimen geometry and test parameter

The dynamic mechanical experiments are performed under the conditions depicted in Table 3.2.

Temperature sweeps were performed with standard tensile specimens according to DIN 53504:2009-10. The used software for the GABO testing system calculates the storage modulus, loss modulus and the loss factor automatically. Further information on the dynamic mechanical analysis is given in Schrittesser [Schrittesser, 2009].

Table 3.2: Overview of used testing parameters used for dynamic mechanical characterization

Testing parameter	Used values
Specimen geometry	3,75mmx2mm
Free clamping length	25mm
Temperature range	-80℃ to 180℃
Heating rate	2℃/min
Mean level	0,5%
Peak to Peak amplitude	0,1%
Frequency	2Hz

3.2.2 Monotonic compression tests

To characterize the time-dependent behavior of the bounded gas and to rank the different materials, compression tests were carried out.

3.2.2.1 Test equipment

For the compression tests a universal testing machine from INSTRON was used (Figure 3.2). A special test set-up was investigated and adapted to the testing machine by Michael Jerabek [Jerabek et al., 2010].

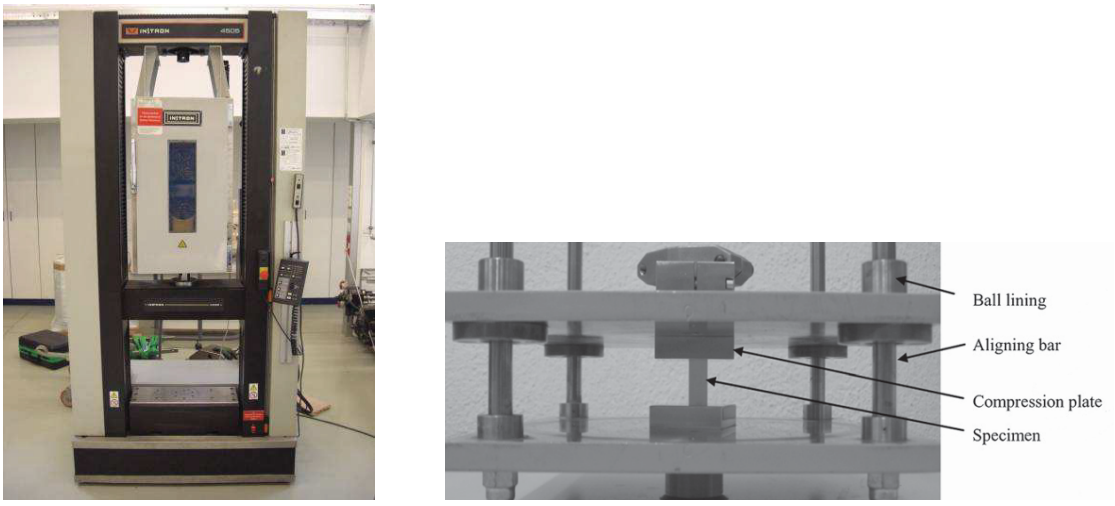

(a) (b)

Figure 3.2: (a) Instron universal testing machine (b) uniaxial compression set-up mounted in the compression tool used for all compression tests [Jerabek et al., 2010]

3.2.2.2 Specimen and test parameter

The same test parameters were applied for the material ranking and the characterization of the time-dependent behavior of the bounded gas. To keep the results comparable with the measured results for constrained specimens, no additional values will be discussed in this thesis. Table 3.3 shows an overview of the used testing parameters. The specimens were cut from a semi-finished product similar to a usual seal. Thus, an equivalent surface roughness was observed for the test specimens as for the finished product [Vezer S.T., in Prog.].

Table 3.3: Overview of the testing parameters used for compression tests

Testing parameter	Used values
specimen geometry	cylindrical Ø8x8mm
temperature	23°C
compression rate	50mm/min
compression	50% strain

3.3 Autoclave tests

As mentioned in chapter 2, different changes can be observed for the material exposed to high pressure gas and high temperature. To be able to catch the whole rapid gas decompression behavior and describe the observed phenomenon information's of each of the following material property classes were necessary:

- Permeation properties of the gas
- Thermal properties of the material
- Deformation behavior of the material
- Fracture behavior of the material

Furthermore, the influence of the pressurization process on the different material properties due to the high pressure gas was necessary. As mentioned, the aim of this study was to implement an instrumented relaxation test set-up to the autoclave testing system and describe the observed behavior. Thus, the discussion of fracture behavior, permeation properties and the thermal properties will be included in further proceedings.

3.3.1 Unconstrained

The whole process will be discussed as a two-step process for unconstrained as well as for constrained investigations. For unconstrained measurements a camera system was implemented to observe the volume change during pressurization and depressurization. This test set-up (Figure 3.3) was investigated in the master thesis by Lederer Klaus [Lederer, 2006].

3.3.1.1 Test equipment

The pressurization and depressurization process were performed on an autoclave test system manufactured by SITEC (Sieber Engineering AG, Zürich, CH). As depicted in Figure 3.3 and mentioned before, a camera system was implemented to measure the volume expansion of the vulcanised rubber.

The test system consisted of a high pressure autoclave, a heating unit and a data acquisition to record the pressure and the temperature during the whole rapid gas decompression process. This test set-up was calibrated for a maximum pressure of 30MPa with a maximum temperature of 145°C. Further, the volume of the autoclave was approximately 500cm^3. Pure CO_2 and CH_4 can be used as well as mixtures of these gases to fill the volume of the autoclave testing system.

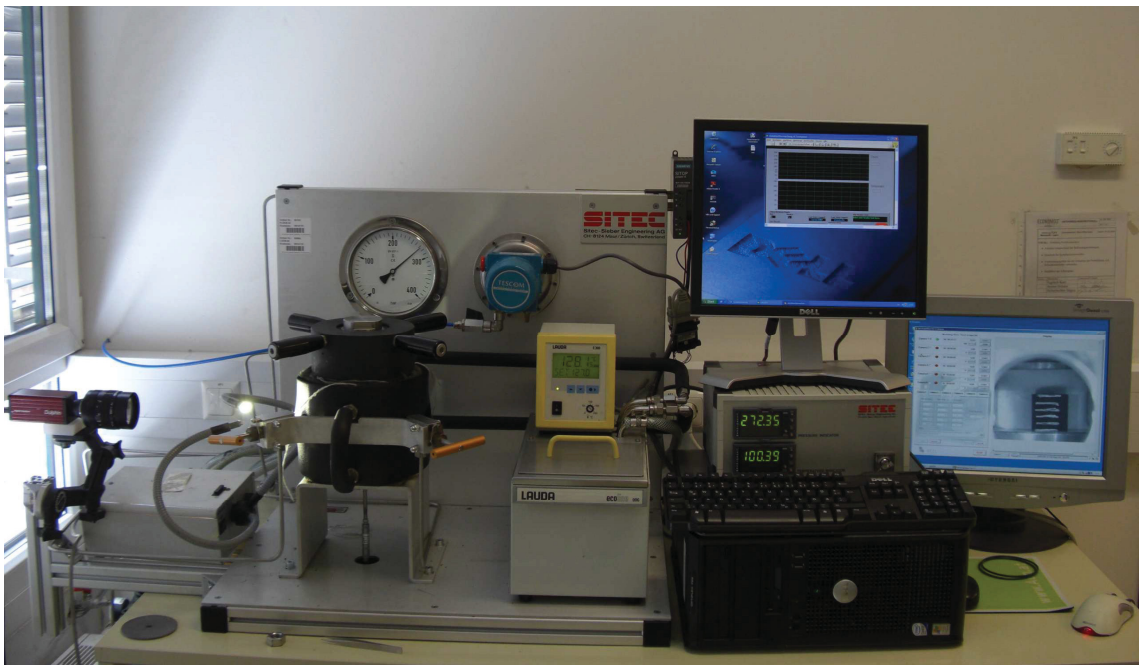

Figure 3.3: Test set-up for unconstrained rapid gas decompression tests

Due to the additional implementation of the camera system, the whole system measured 3 parameters during the test procedure:

- temperature,
- pressure,
- volume change.

Basically, diverse unconstrained test set-ups for cylindrical specimens or whole seals could be conducted.

3.3.1.2 Test parameters

Ambient gas

The unconstrained measurements were exposed to pure CO_2, because of the higher influence on the properties, as discussed in chapter 2.

Ambient pressure

Since a comparison of unconstrained and constrained measurements should be implemented in this thesis, the maximum pressure was restricted by the relaxation test set-up. However, the used test pressure for this thesis was 15MPa.

Temperature

For the same reason as for the pressure, a similar constriction was used resulting in a maximum temperature of 60°C.

Decompression time

Because the test set-up required a manual opening of the decompression valve, the minimal decompression time was restricted to 20 seconds to empty the whole vessel, exposed to a maximum pressure of 30MPa.

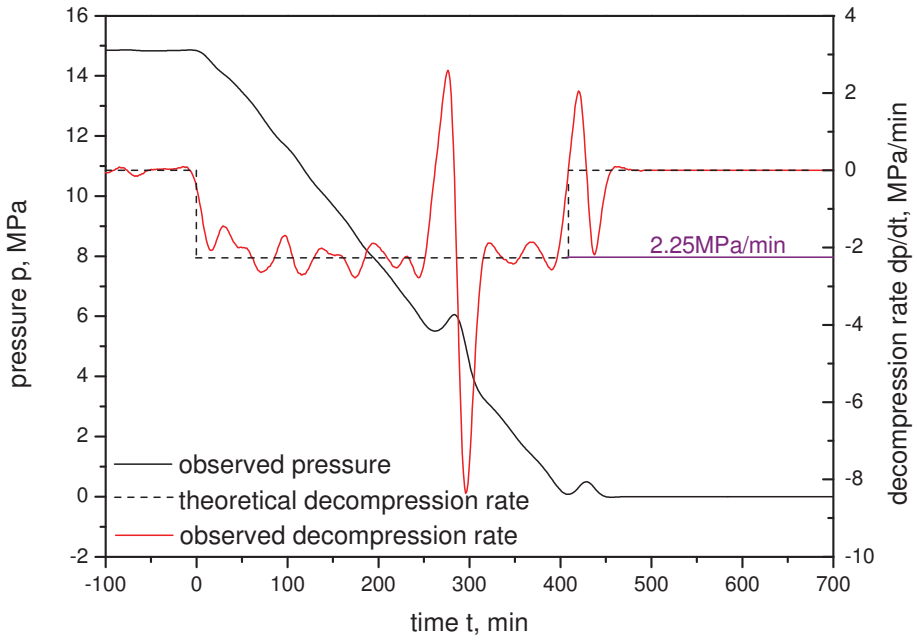

Figure 3.4: Pressure/decompression rate in dependence of time

For the tests performed in this thesis the decompression rate was fixed to a constant value of 2.25MPa/min. As depicted in Figure 3.4 small fluctuations of the decompression rate were observed, due to the manual opening of the decompression valve.

Exposure time

Considering the literature [NACE, 2003, NORSOK, 2001] single cycle test as well as multi-cycle tests were documented. To keep this thesis in an acceptable frame, the discussed unconstrained measurements were conducted at an exposure time of 15 hours.

Test specimen

To provide the visual observation with a camera system, cylindrical specimens (diameter 8mm, height 8mm) were used. Figure 3.5 compares typical images recorded by the camera system at the start of pressurization (a), depressurization (b) and at end of the depressurization phase (c).

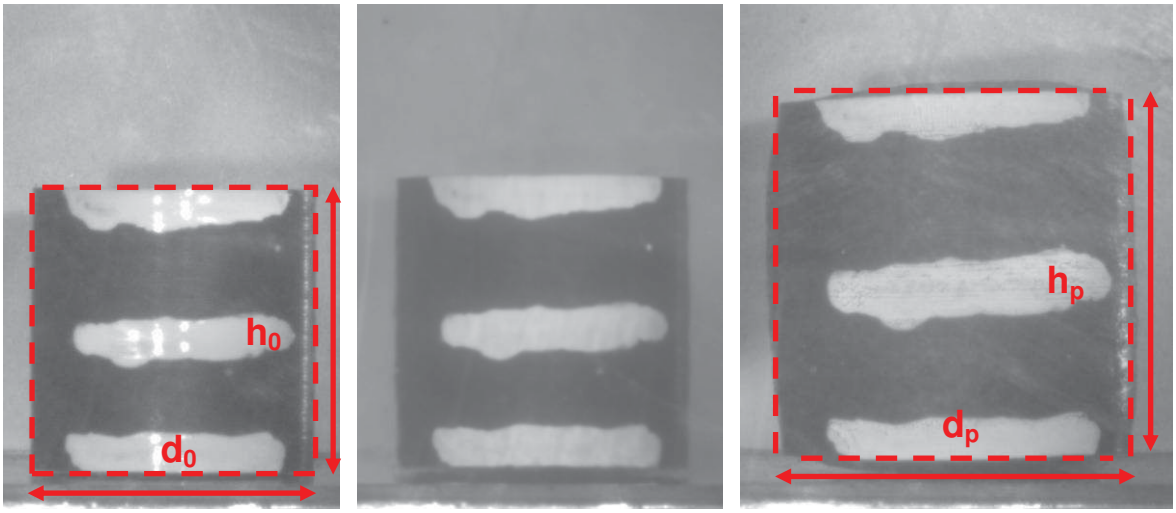

(a) (b) (c)

Figure 3.5: Specimen at the start of the (a) pressurization, (b) depressurization and (c) at the end of the depressurization phase

First of all, the specimen diameter d_0 and height h_0 were measured. Afterwards, the camera system was calibrated to these values, as depicted in Figure 3.5 (a).

$$V_i = \frac{d_i^2 \cdot \pi}{4} \cdot h_i \tag{XVIII}$$

During the depressurization process a large volume increase was observed combined with barrelling of the specimen. A linear approximation was performed to reduce the influence of the barrelling on the height and the diameter. Finally, the volume was calculated, using equation (XVIII), and compared with the start volume.

3.3.2 Constrained

As mentioned in the introduction, the main aim of this thesis was to implement a constrained test set-up to the autoclave testing system. To perform the next step towards a scientific characterization near the application, the implementation of constrained measurements was necessary. For the investigation of material modelling in future proceedings, in-situ measurements of the mechanical properties were required. Thus, a relaxation test set-up was constructed and implemented.

3.3.2.1 Test equipment

Several components were necessary to realize a relaxation test set-up inside a high pressure vessel:

- Mechanical component of the relaxation test set-up,
- Load cell,
- Radio system.

Because of the restricted available volume in the vessel, the size of the mechanical component and the specimen geometry was limited. Moreover, the exposure to a high pressure regime seemed to be difficult, but not impossible.
The design of the mechanical component is depicted in
Figure 3.6. There are four guiding pins between a bottom and a cover plate guiding a cross head. This cross head was mechanically fixed before the test. Further, the cross head comprised the load cell (KALIBER Kft, Hungary) which was connected to the radio system. To realize the implementation of cylindrical specimens and whole seals, the bottom plate of the relaxation test set-up was modified (Figure 3.6 a,b).

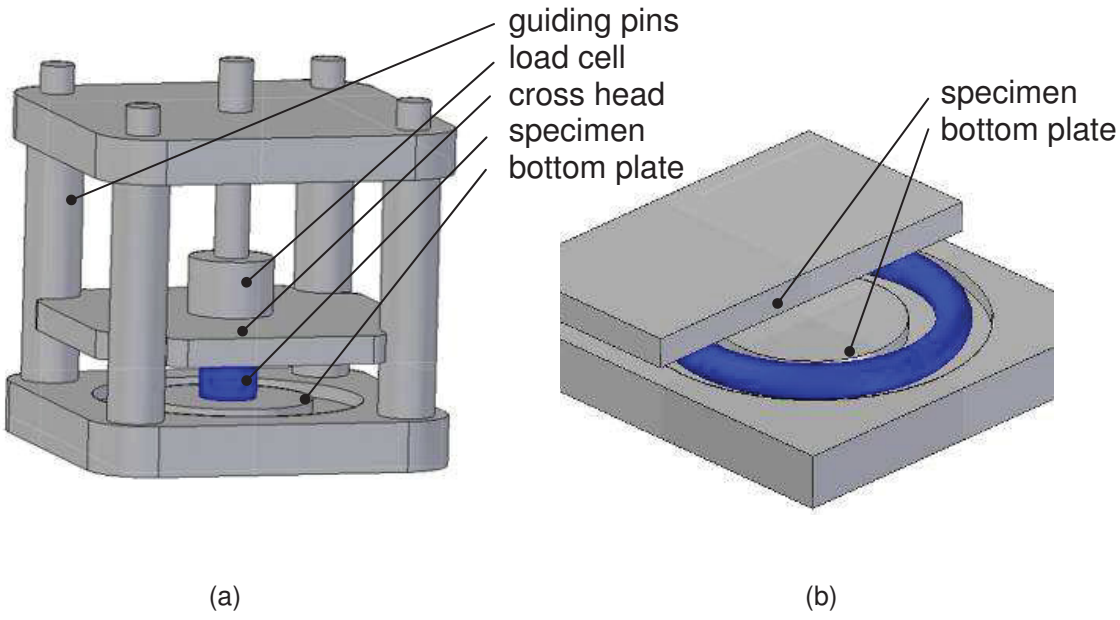

Figure 3.6: Mechanical component of the relaxation test set-up for cylindrical specimens/whole seals

The radio system was constructed and manufactured by MANNER Sensortelemetrie GmbH (Spaichingen, Germany). As shown in Figure 3.7, the system consisted of a radio receiver and a radio transmitter. The radio transmitter was directly fixed to the load cell and implemented in the vessel. To record the signal outside the autoclave, the radio receiver was connected to a second data acquisition unit. The complete test set-up is depicted in Figure 3.8.

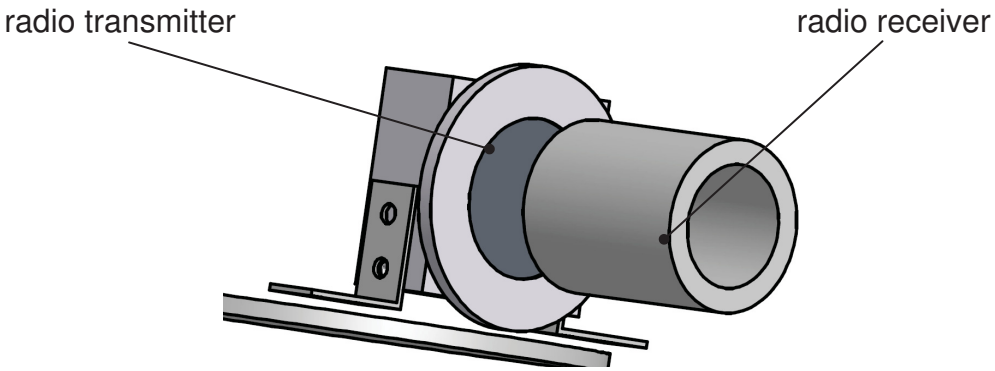

Figure 3.7: Radio system for the relaxation test set-up

Because of the limited volume of the vessel, a classical calibration of the relaxation test set-up was not possible. Thus, the influences on the test set-up were recorded and will be discussed on the next pages.

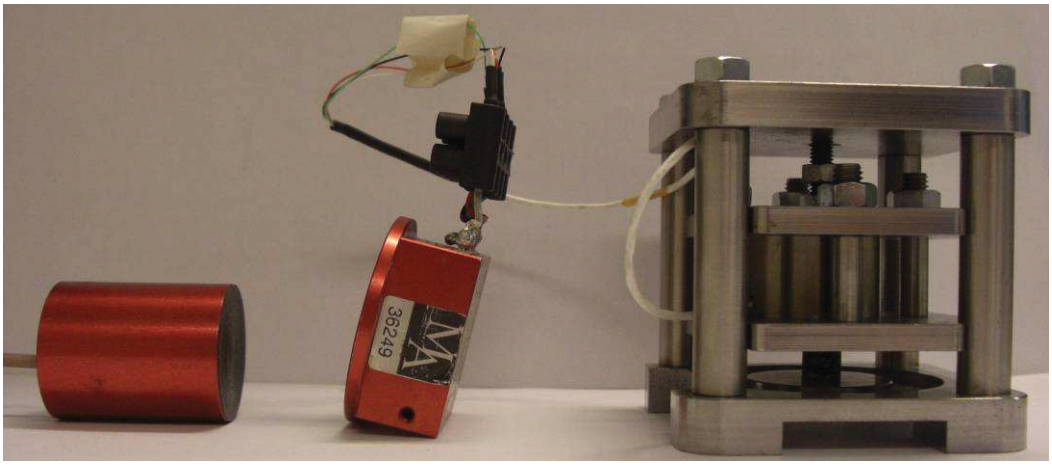

Figure 3.8: Test set-up for constrained measurements with remote system

The first interesting aspect is the time stability of the whole system. As depicted in Figure 3.9, the influence of the time on the test set-up (maximum 6mV) is not mentionable. The depicted curve was measured at room temperature and at

atmospheric pressure. As second part, the influence of the test temperature was investigated. Figure 3.10 shows a clear dependence of the test set-up for the first hours resulting in an equilibrium. This indicates the temperature dependence of the load cell and the radio system. Since preconstrained specimens should be tested as well, a calibration curve was necessary.

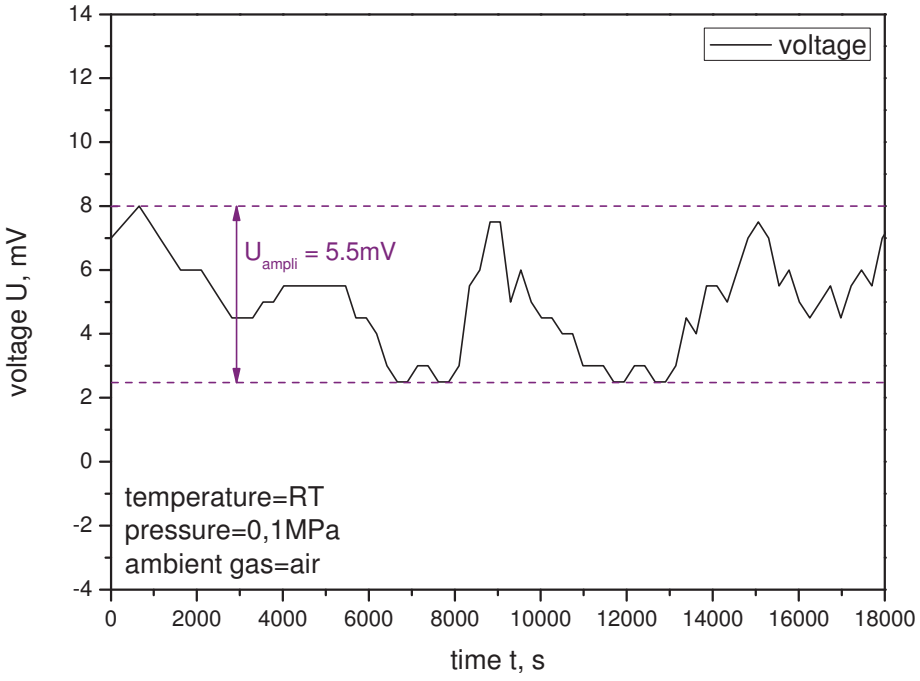

Figure 3.9: Time stability of the test set-up at room temperature

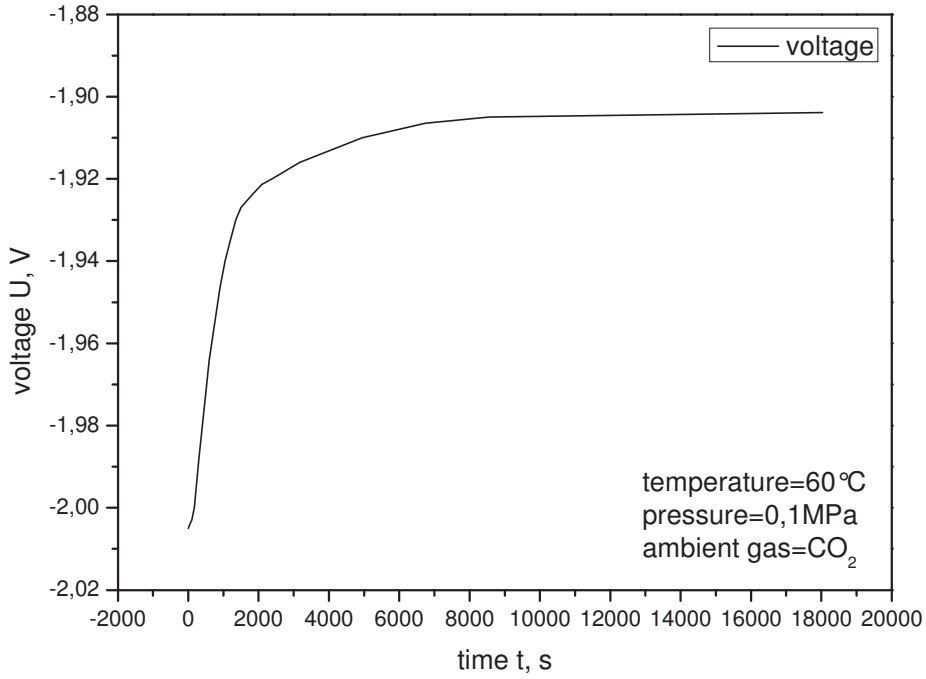

Figure 3.10: Time stability of the test set-up at 60°C

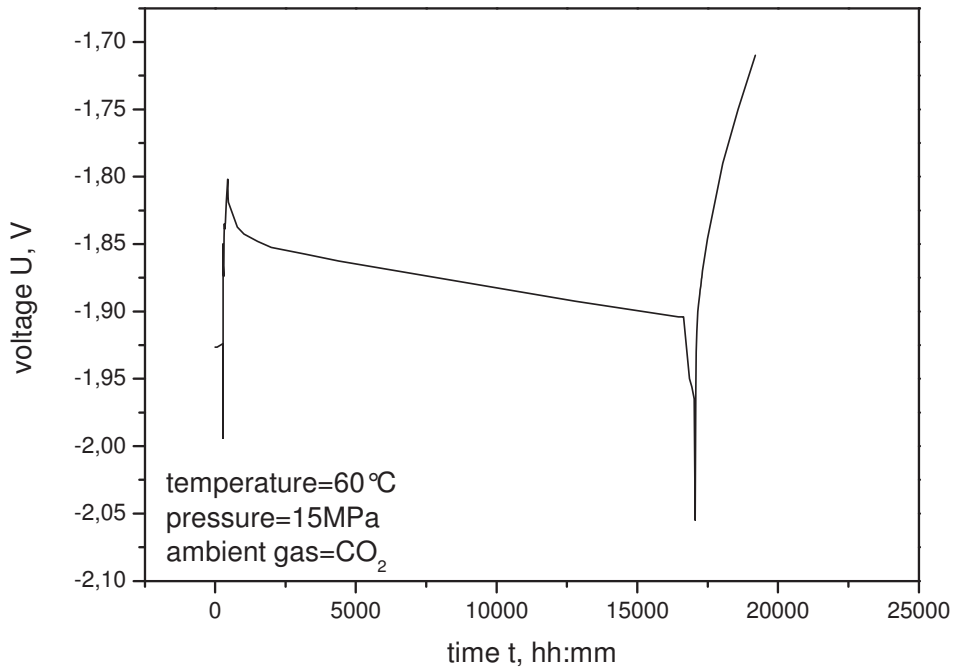

Figure 3.11: Response of the measurement system without specimen, in gas

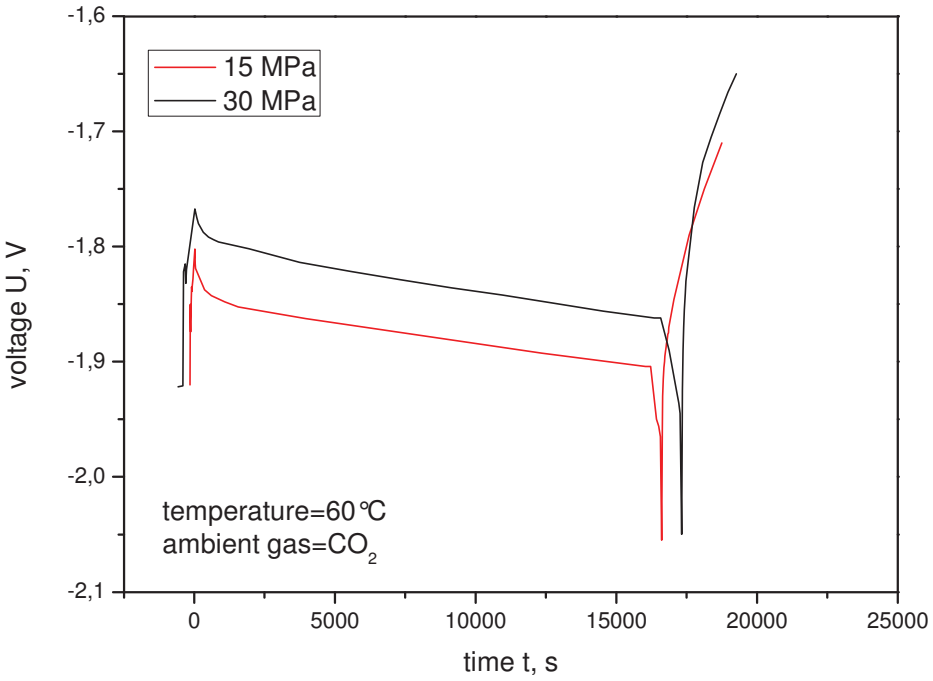

Figure 3.12: Comparison of two calibration measurements at 15MPa and 30MPa

Furthermore, the pressure also strongly influenced the test set-up as depicted in Figure 3.11. Thus, a defined time schedule was compared with calibration measurements. These calibration measurements were subtracted of each recorded curve afterwards to receive the material behavior.

In Figure 3.12, the calibration curve for 15MPa and 30MPa is shown. As depicted, the observed curve for 30MPa was shifted to higher values. Furthermore, a bigger influence during depressurization was achieved. Due to the constant depressurization rate, the time for the decompression increased.

The previously mechanical compression of the specimen with the novel test set-up is depicted in Figure 3.13. This compression results in a maximum signal increase (ΔU) at a strain value of 25%. Furthermore, compression tests were carried out at a maximum strain value of 50%, using an INSTRON testing system (Chapter 3.2.2). The observed force for 25% strain is shown in Figure 3.14. Due to the previous mechanical compression of the specimen to a maximum strain of 25%, the voltage signal (novel test set-up) could be compared with the force observed for the 25% of compression (INSTRON testing system). Thus, a relation between

the “signal in mV” and the “force in N” was found. Using this correlation, the recorded signal of the remote system could be recalculated.

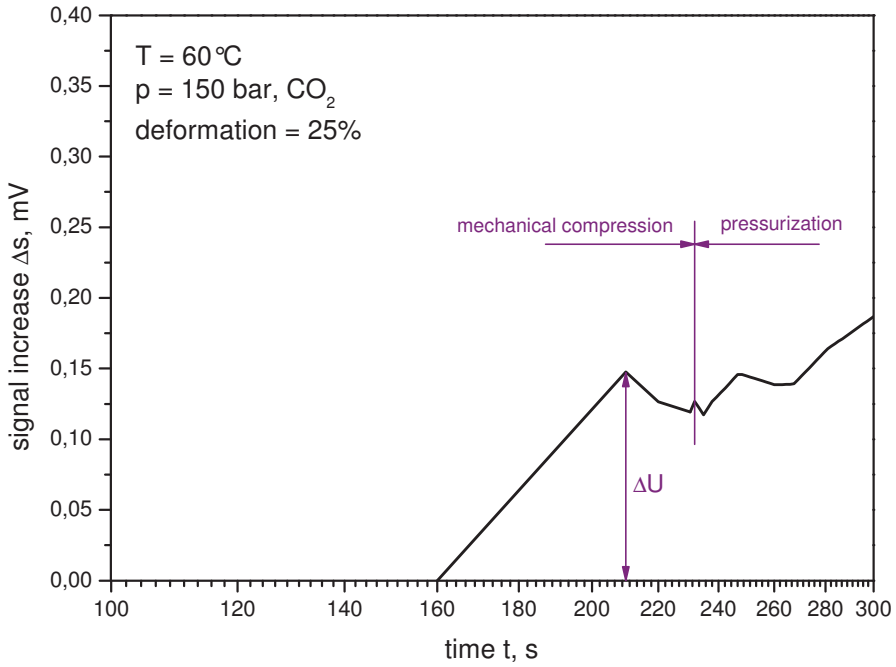

Figure 3.13: The signal increase of the remote system with constrained specimen in dependence of the time

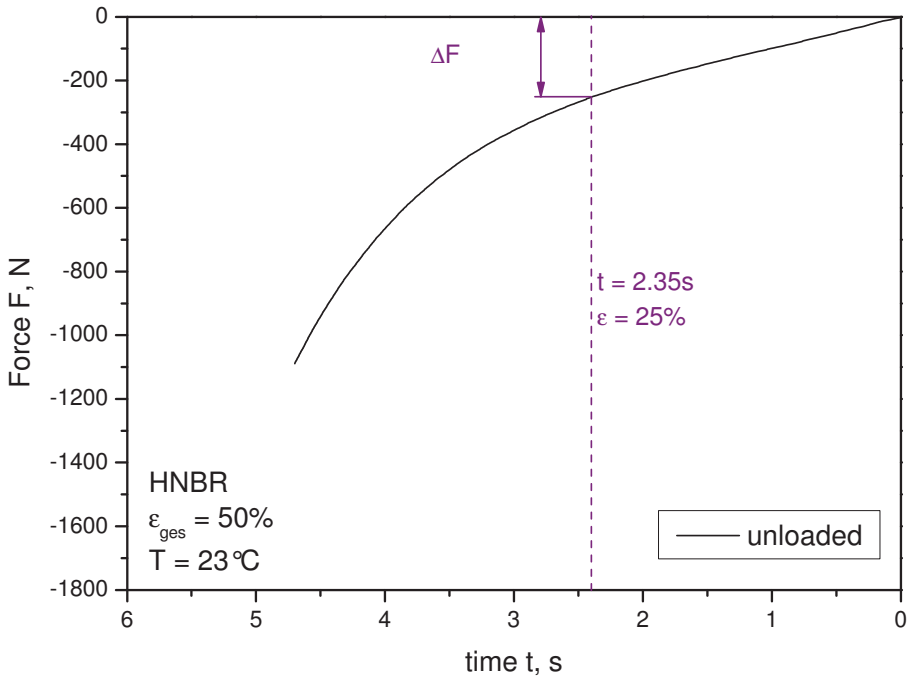

Figure 3.14: Force in dependence of the displacement for HNBR

3.3.2.2 Testing parameter

To compare the constrained measurements with the unconstrained measurements, most of the parameters were kept at the same value as for the unconstrained records. Further, similar specimens (cylindrical, diameter 8mm, height 8mm) were used. These specimens were previously pre-constrained to 6mm height (25% compression) before the pressurization process started. Table 3.4 summarizes the used testing parameters where only the exposure time was varied to 5 hours in comparison to unconstrained experiments.

Table 3.4: Overview of used specimens for unconstrained and constrained measurements

Testing parameter	Unconstrained	Constrained
Ambient gas	CO_2	CO_2
Pressure	15Mpa	15MPa
Temperature	60℃	60℃
Decompression rate	2,25MPa/min	2,25MPa/min
Exposure time	15 hours	5 hours
Specimens	Cylindrical Diameter: 8mm Height: 8mm	Cylindrical Diameter: 8mm Height: 8mm

3.4 Data reduction

Due to the high amount of produced data, the measured curves were reduced to three specific values:

- maximum volume (Figure 3.15) / force change (Figure 3.17) during pressurization at saturation (about +-1% difference in 100s),
- maximum volume (Figure 3.16) / force change (Figure 3.18) during depressurization,
- maximum temperature change during depressurization for unconstrained (Figure 3.16) and constrained (Figure 3.18) measurements,
- the incubation time between the start of the depressurization phase and the start of the volume (Figure 3.16)/force change (Figure 3.18).

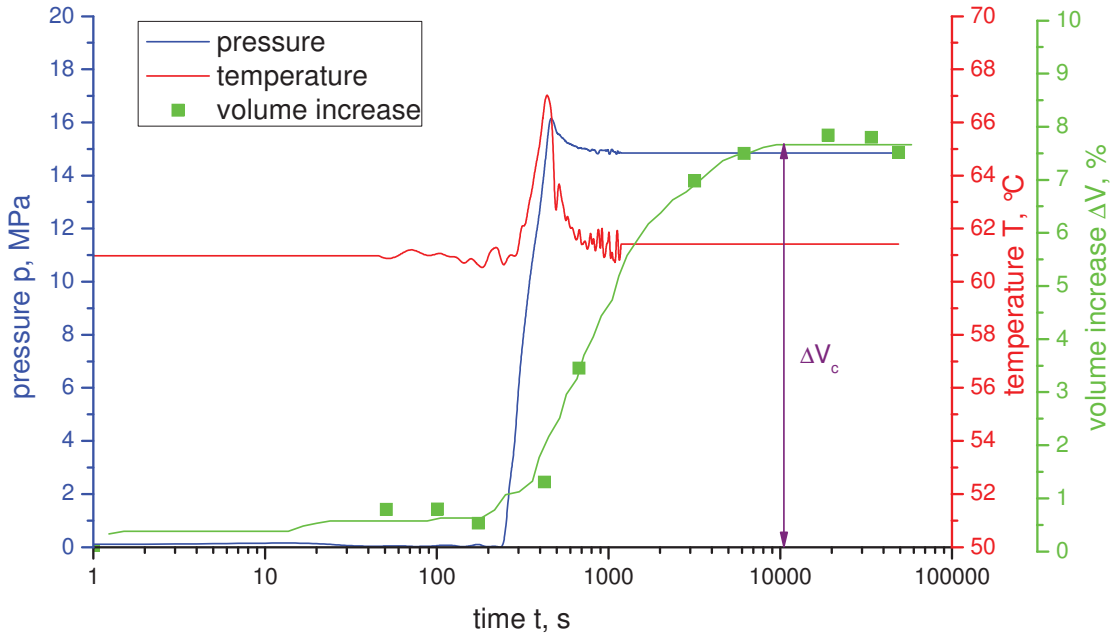

Figure 3.15: Volume increase ΔV_c during the pressurization phase, unconstrained

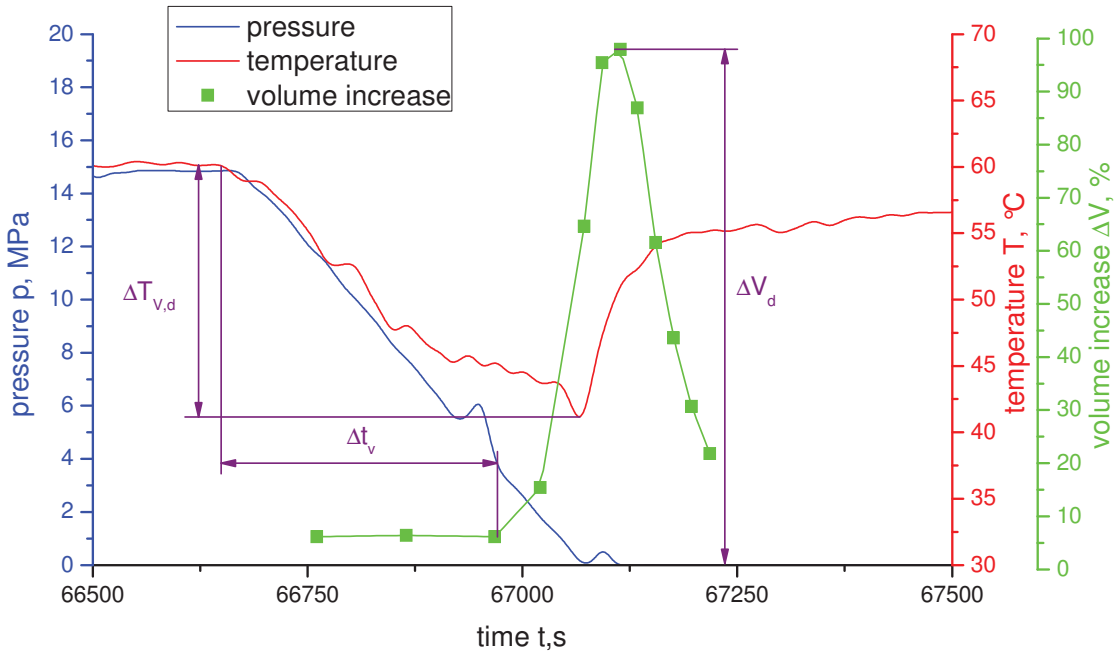

Figure 3.16: Volume increase ΔV_d, temperature decrease $\Delta T_{V,d}$ and incubation time Δt_V during the depressurization phase, unconstrained

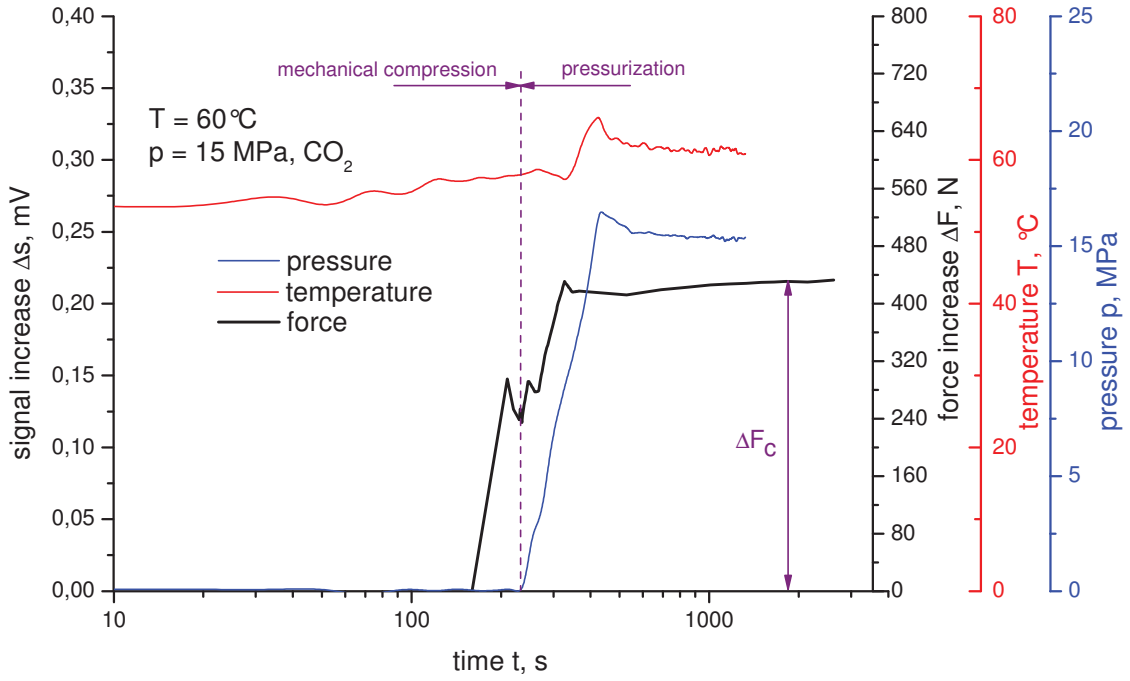

Figure 3.17: Force increase ΔF_c during the pressurization phase, constrained

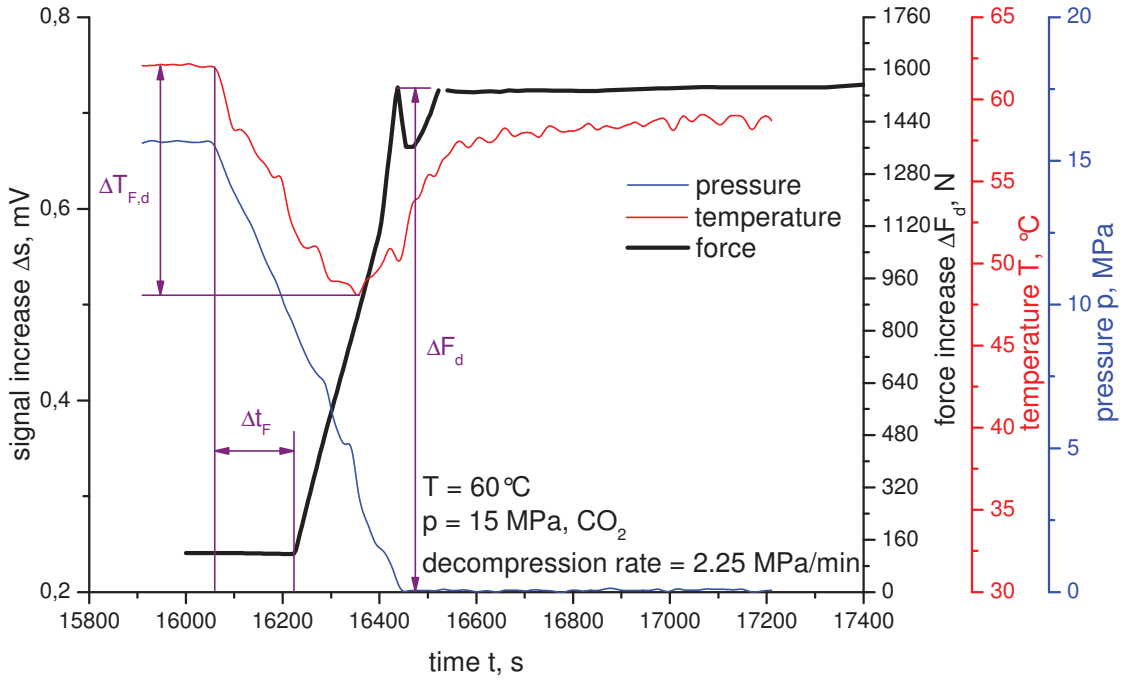

Figure 3.18: Force increase ΔF_d, temperature decrease $\Delta T_{F,d}$ and incubation time Δt_F during the depressurization phase, constrained

Table 3.5: Comparison of characteristic values

	Unconstrained	Constrained
Compression	volume increase at saturation ΔV_c	force increase at saturation ΔF_c
Decompression	max. volume increase ΔV_d	max. force increase ΔF_d
	time to volume increase Δt_v	time to force increase Δt_F
	max. temperature difference $\Delta T_{v,d}$	max. temperature difference $\Delta T_{F,d}$

Table 3.5 shows an overview of the characteristic values, used for the comparison of the different materials. In order to better characterize the influence of filler and the ACN content on the rapid gas decompression performance during the compression and the decompression phase, the following quantities were defined and calculated (Figure 3.19).

Figure 3.19: Relation between the experimental materials and the filler/ACN factor

The filler factor describes the influence of the additional filler for unconstrained and constrained measurements. Basically, three different filler factors were built for each test set-up. The first, $Filler_C$, described the effect on the volume/force change during the compression phase. Therefore, the volume/force change of HNBR1 and HNBR at saturation was divided (equation (XIX)).

$$Filler_c = \frac{\Delta V_{HNBR1,c}}{\Delta V_{HNBR,c}} = \frac{\Delta F_{HNBR1,c}}{\Delta F_{HNBR,c}} \tag{XIX}$$

$Filler_D$ specified the influence of additional filler during the decompression phase in the same way (equation (XX)).

$$Filler_d = \frac{\Delta V_{HNBR1,d}}{\Delta V_{HNBR,d}} = \frac{\Delta F_{HNBR1,d}}{\Delta F_{HNBR,d}} \tag{XX}$$

Moreover, to determine the influence on the incubation time the third factor, $Filler_{t\Delta V}$/$Filler_{t\Delta F}$, was attached.

$$Filler_{t\Delta V} = \frac{\Delta t_{HNBR1,d\Delta V}}{\Delta t_{HNBR,d\Delta V}} \quad \text{(XXI)}$$

$$Filler_{t\Delta F} = \frac{\Delta t_{HNBR1,d\Delta F}}{\Delta t_{HNBR,d\Delta F}} \quad \text{(XXII)}$$

In a similar way, the ACN factor was set up. These factors characterize the effect of the acrylonitrile content for unconstrained and constrained measurements. The ACN_C depicts the effect of the rising acrylonitrile content on the volume/force change during pressurization (equation (XXIII)).

$$ACN_c = \frac{\Delta V_{HNBR2,c}}{\Delta V_{HNBR1,c}} = \frac{\Delta F_{HNBR2,c}}{\Delta F_{HNBR1,c}} \quad \text{(XXIII)}$$

The second factor, ACN_D, describes the influence of the higher acrylonitrile content on the volume/force change during the decompression phase (equation (XXIV)).

$$ACN_d = \frac{\Delta V_{HNBR2,d}}{\Delta V_{HNBR1,d}} = \frac{\Delta F_{HNBR2,d}}{\Delta F_{HNBR1,d}} \quad \text{(XXIV)}$$

As displayed in equations (XXV) and (XXVI), the $ACN_{t\Delta V}/ACN_{t\Delta F}$, determines the manipulation of the rising acrylonitrile content for the incubation time.

$$ACN_{t\Delta V} = \frac{\Delta t_{HNBR2,d\Delta V}}{\Delta t_{HNBR1,d\Delta V}} \quad \text{(XXV)}$$

$$ACN_{t\Delta F} = \frac{\Delta t_{HNBR2,d\Delta F}}{\Delta t_{HNBR1,d\Delta F}} \quad \text{(XXVI)}$$

4 RESULTS AND DISCUSSION

4.1 Material characterization

4.1.1 Dynamic mechanical analyses

Dynamic mechanical analyses were conducted to observe the performance of the modulus in dependence of the temperature. Furthermore, the influence of the rising acrylonitrile content was investigated. In Figure 4.1, the dependence of the storage modulus with rising temperature is depicted.

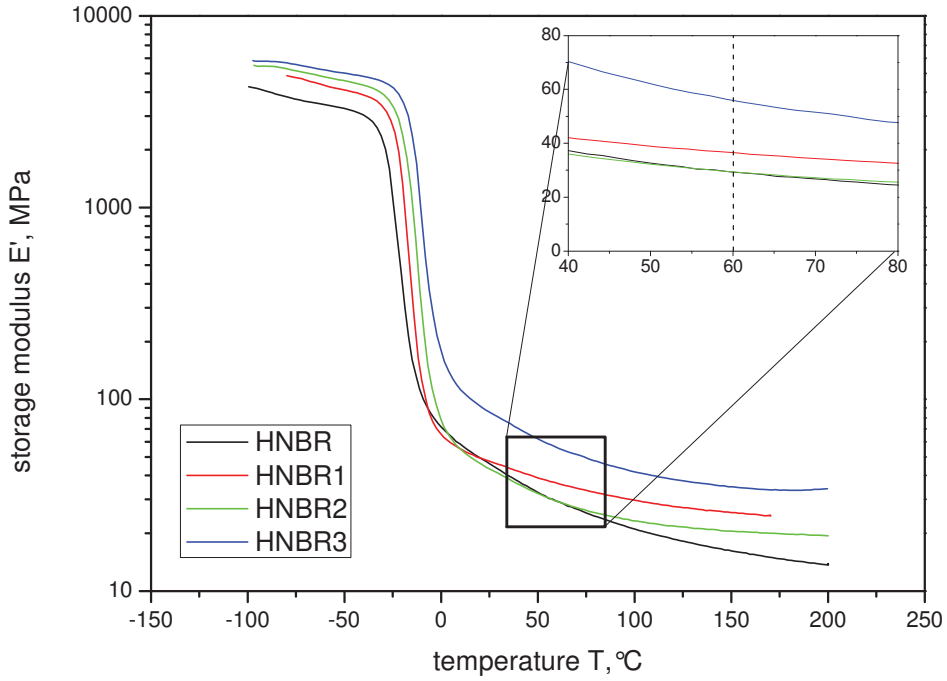

Figure 4.1: The storage modulus in dependence of the temperature for tested materials

As expected, the rising acrylonitrile content resulted in a shift of the glass transition temperature to higher values (from –25 °C for HNBR to –5 °C for HNBR3). An interesting material behavior was observed for higher temperatures. Especially for 60 °C, the order of the material changed, due to the different slope of the curves after the glass transition temperature. By comparing HNBR and HNBR1 a clear influence of the rising acrylonitrile content was observed. Regarding literature [Sommer and Röthemeyer, 2006], increasing acrylonitrile content shifts the glass

transition temperature to higher values. Furthermore, a higher modulus was observed with increasing temperature. This indicates a harder material performance for HNBR1. With the additional filler contained in HNBR2, the glass transition temperature rises. In contrast to the observed material performance with increasing acrylonitrile content the material performs in a softer way at higher temperatures. HNBR3 includes both effects, resulting in a higher glass transition temperature and a harder material performance for increasing temperature.

4.1.2 Monotonic compression tests

For the comparison of the different test set-ups, compression tests were performed. Furthermore, the influence of the time after the depressurization process was investigated.

4.1.2.1 Monotonic compression test after different times

One important aspect of the characterization of the materials with compression tests is the influence of the time after the depressurization phase. Therefore, compression tests were conducted with varying time spans between the end of the pressurization process and the start of the compression test. Figure 4.2 shows this time dependent behavior for HNBR.

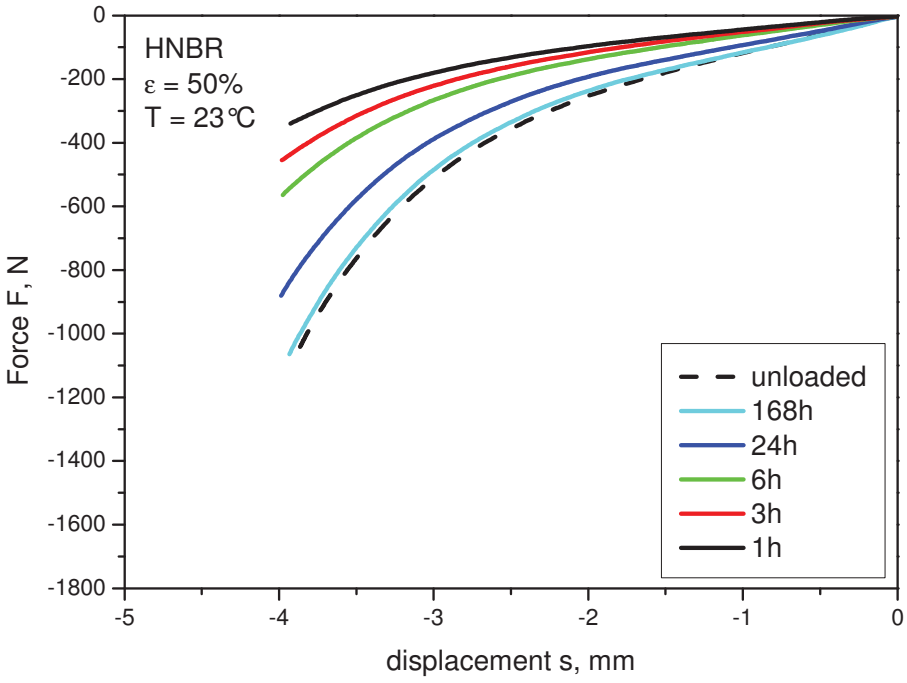

Figure 4.2: Influence of the time span on the compression performance of HNBR

The dashed line represents a virgin test specimen. As depicted, the compression curve of HNBR with time nearly reaches the virgin curve in tests realized 168 hours after depressurization. As shown in Figure 4.3 and Figure 4.4, HNBR1 and HNBR2 showed a similar behavior regarding HNBR.

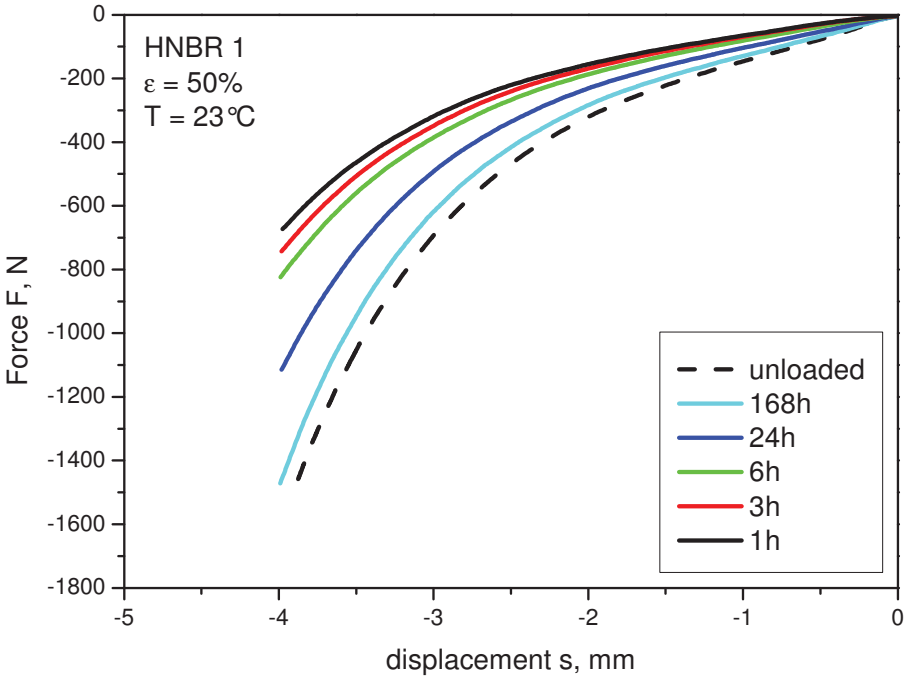

Figure 4.3: Influence of the time on the compression performance of HNBR1

HNBR1 depict a slight difference between the virgin curve and the compression performance after 168 hours. This indicates that the additional filler increases the effective diffusion length of the material and locks the bounded gas longer in the material than HNBR [Amerongen, 1964]. The rising acrylonitrile content seems not to influence the diffusion performance of the material. Therefore, HNBR2 depict a slight difference between the virgin curve and the compression performance after 168 hours. The difference between HNBR1 and HNBR2 is the softer compression performance of HNBR2. This softer material performance fits to the smaller storage modulus of HNBR2 with rising temperature.

Figure 4.5 indicates that the filler added to HNBR3 strongly influences the diffusion performance of the material. Furthermore, the highest storage modulus for HNBR3 during the dynamic mechanical characterization results in a much harder material performance during the compression test.

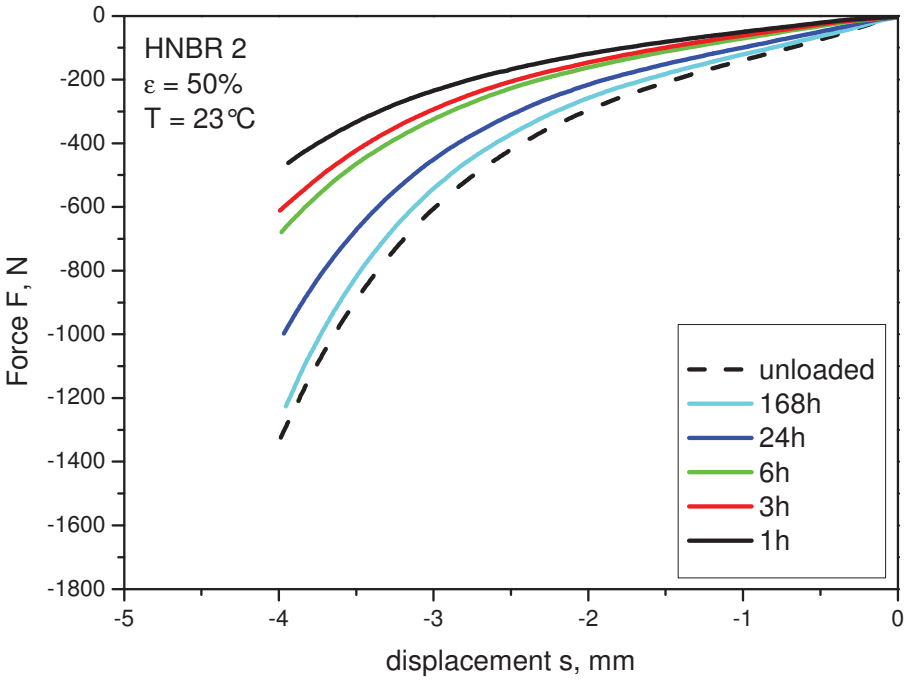

Figure 4.4: Influence of the time span on the compression performance of HNBR2

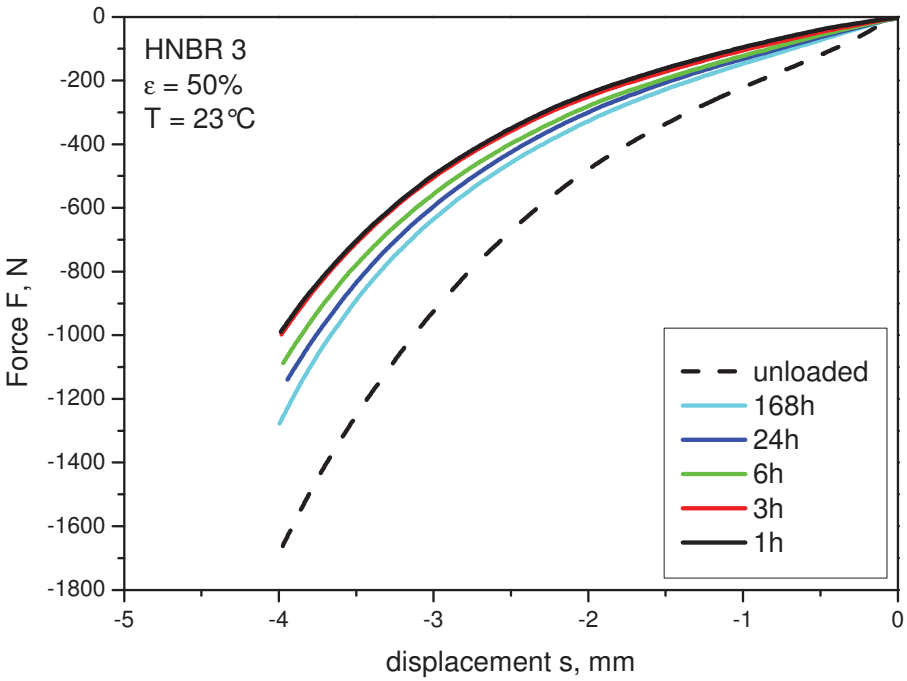

Figure 4.5: Influence of the time span on the compression performance of HNBR3

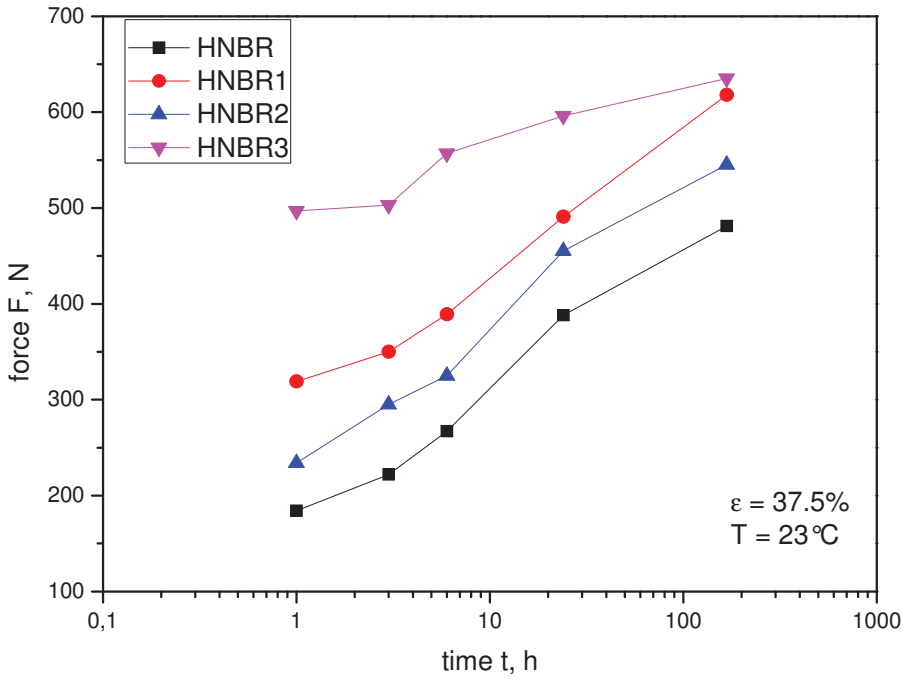

Figure 4.6: Increase of the force in dependence of time for 37.5% strain

In Figure 4.6 the increase of the force for a deformation of 37.5% in dependence of time is depicted. As mentioned before, HNBR, HNBR1 and HNBR2 showed slight differences in the diffusion performance. HNBR3 showed a much slower force increase with time. Further investigations with longer time spans (up to 500 hours) are necessary to characterize the dependence of this process.

4.1.2.2 Monotonic compression tests with unloaded, unconstrained and constrained specimens

Compression tests were carried out to investigate the influence on the material performance for different test set-ups. Overall, two different test set-ups unconstrained and constrained ones, and the virgin curve were used for the material characterization.

Figure 4.7 shows the performance curve of the tested materials up to a maximum strain of 50%. The dashed line represents the material behavior of unconstrained specimen. Due to the exposure to high pressure gas and temperature, the material started a secondary vulcanisation, thus resulting in an increasing force in dependence of time. The constrained measurement, depicted with dots, show a

similar behavior to the virgin curve for small strains. For higher deformation the constrained curve reaches the unconstrained curve and results finally in higher force for deformations larger than 45% strain.

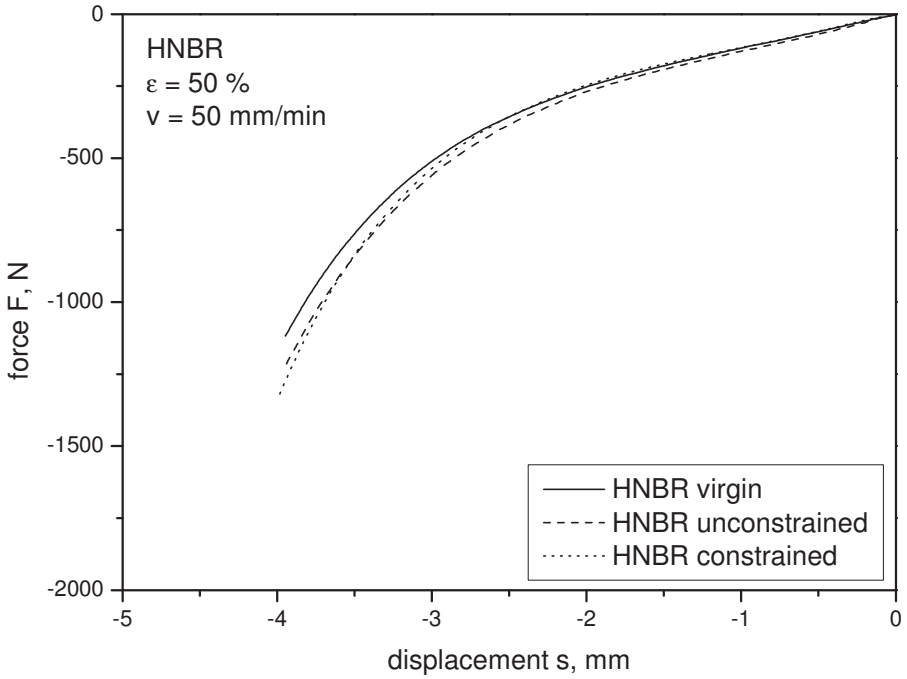

Figure 4.7: Force in dependence of the displacement for HNBR virgin, unconstrained and constrained test set-ups

This observed behavior for HNBR changed for HNBR1. Based on the higher storage modulus of the material, HNBR1 showed a small force increase for the virgin curve. The shift between the compression performances of unconstrained specimens was also shown for HNBR1, but in another direction (Figure 4.8). This shift indicates that the filler added to the material produced a particulate separation of the filler surface and the vulcanised rubber. Hence, a decrease of the compression performance for the material was observed. The compression behavior for constrained specimens showed similar values for small strain values. With increasing strain the slope of the curve increased too and reached the virgin curve for deformations over 50%. Thus, an increase of the acrylonitrile content seemed to perform better for higher strain values.

Figure 4.9 shows the force in dependence of the deformation for HNBR2. The increase of the acrylonitrile content resulted in a shift to higher values for the

compression performance. Therefore, the different test set-ups resulted in nearly the same value for HNBR2.

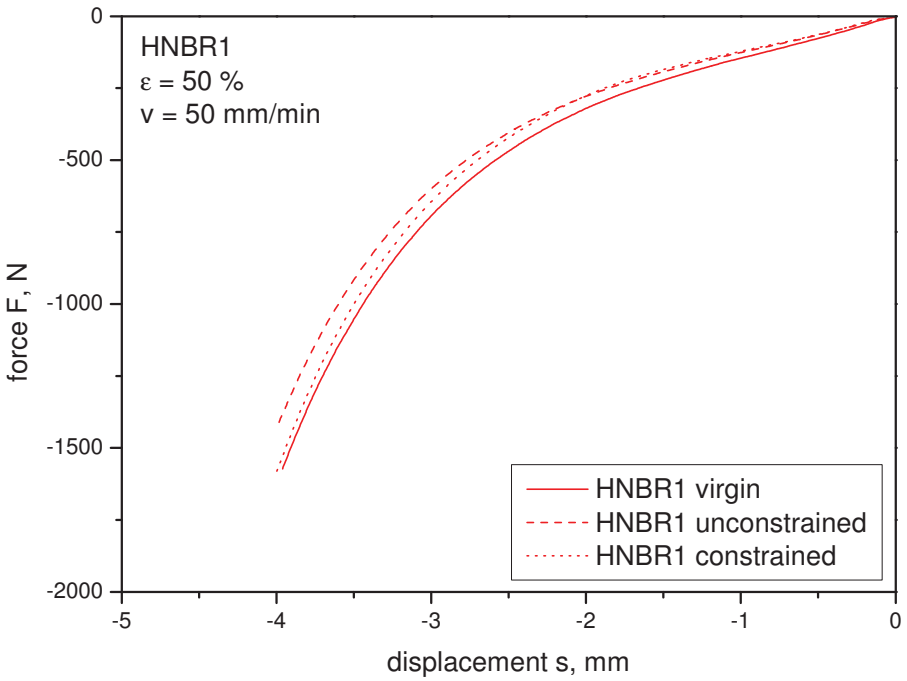

Figure 4.8: Force in dependence of the displacement for HNBR1 virgin, unconstrained and constrained test set-up

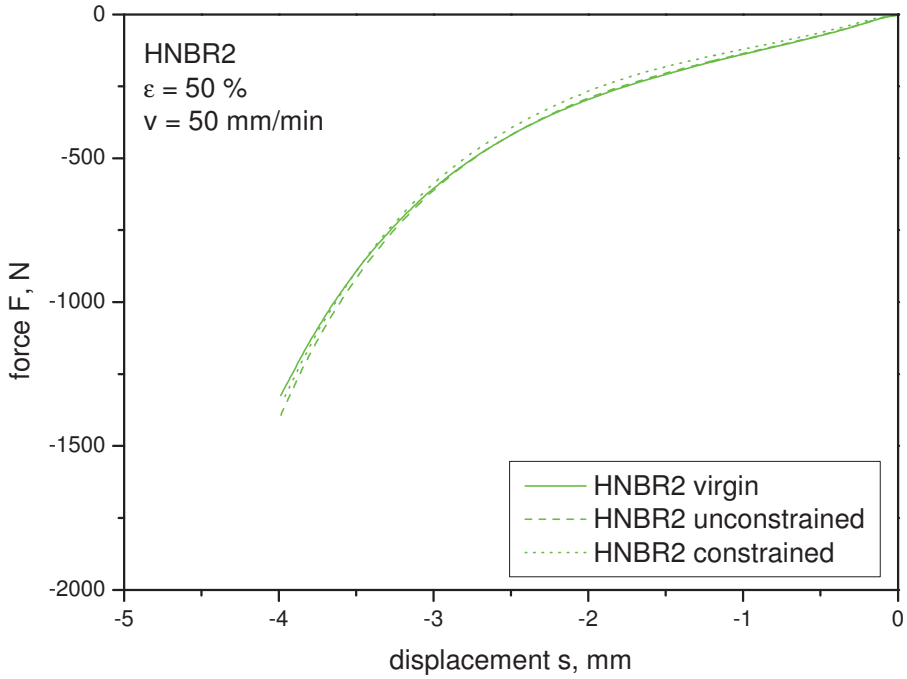

Figure 4.9: Force in dependence of the displacement for HNBR2 virgin, unconstrained and constrained test set-up

As depicted in Figure 4.10, the additional filler in HNBR3 acted similarly to the influence of the filler on HNBR1. In general a softer material behavior was observed for the material performance This indicates a higher damage grade in the material with adding additional fillers and goes along with the results discussed before.

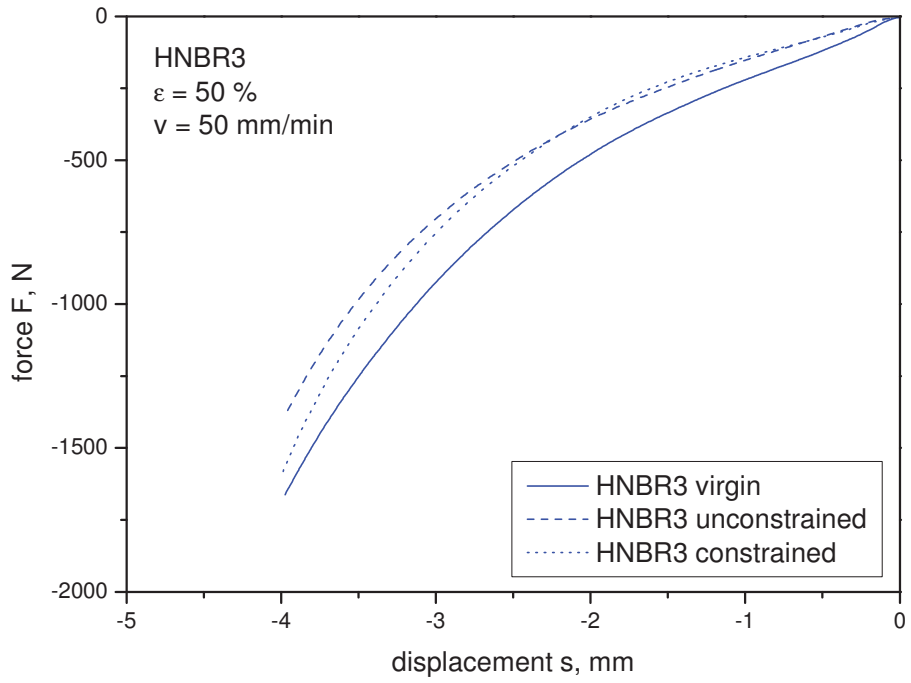

Figure 4.10: Force in dependence of the displacement for HNBR3 virgin, unconstrained and constrained test set-up

In order to compare the tested materials, the results are summarized and depicted at a specific deformation value (x=3mm) in Figure 4.11. As mentioned, the performance for the virgin specimens (unloaded) matched the results observed for the dynamic mechanical investigations. HNBR acted as the softest material in direct comparison. Due to the additional filler, HNBR1 showed an increase of the force. A small drop was observed with rising acrylonitrile content for HNBR2 followed by a rising force for HNBR3, because of the additional filler. Furthermore, the values for unconstrained and constrained specimens seemed comparable with similar tendencies. The additional filler in HNBR1 resulted in a decrease of the observed volume/force for unconstrained and constrained test set-ups. With rising acrylonitrile content the values for unconstrained and constrained nearly reached

the virgin curve, which indicates a decreasing filler matrix separation for HNBR2. To desribe the performance of HNBR3 further experiments are necessary.

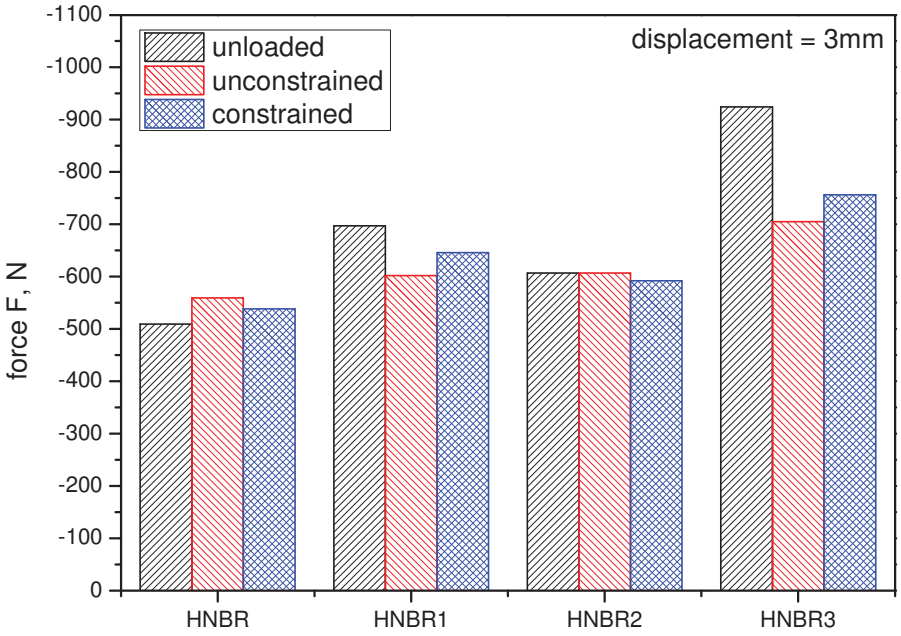

Figure 4.11: Comparison of the observed forces for tested materials with virgin, unconstrained and constrained test set-ups

4.2 Autoclave tests

Basically, two different test set-ups were used for the characterization of the material performance with the autoclave testing system. Unconstrained measurements were carried out to investigate the volume increase. Furthermore, the increase of the uniaxial force for constrained measurements was recorded.

4.2.1 Unconstrained

As mentioned before, the test process consists of a compression phase and a decompression phase. These two phases were separated for both test set-ups and will be discussed separately.

In Figure 4.12 the volume increase for the compression and the decompression phase is depicted. The used material in this experiment was HNBR. This curve represents a representative measurement which was investigated for unconstrained measurements.

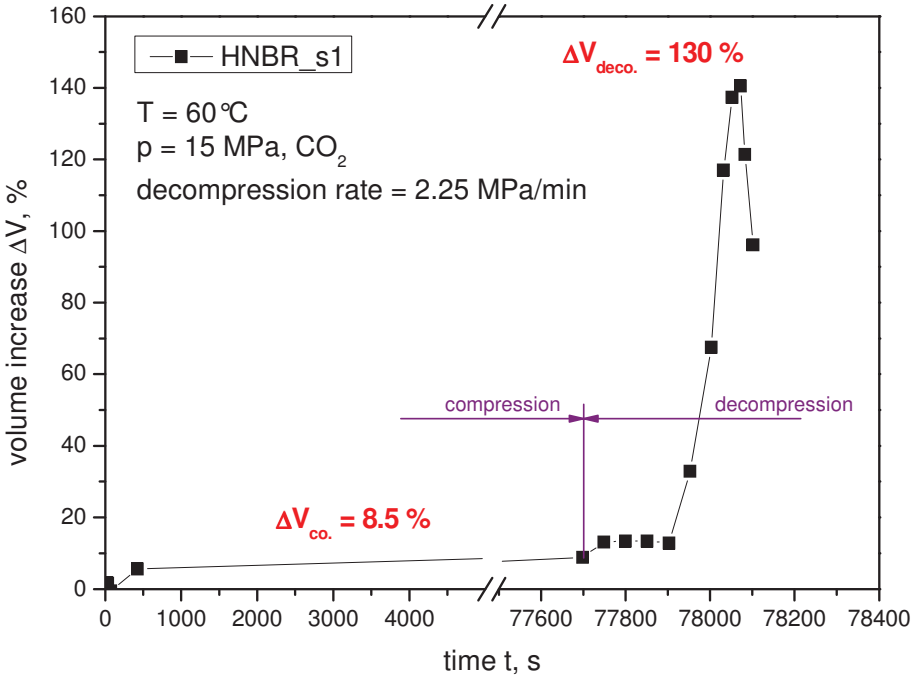

Figure 4.12: Observed volume increase during the compression and decompression phase

4.2.1.1 Compression (saturation ΔV_c)

The high temperature and the high pressure caused a material saturation by the ambient gas. This penetration phase depends on the material properties, the ambient gas and the temperature. Because of the saturation, equilibrium was reached after some time (Figure 4.13). Due to the increasing pressure, the saturation phase started with the pressurization process.

An unstable situation was generated with increasing pressure. It took some specific time to reach equilibrium for the temperature and the pressure after the end of the pressurization process. This specific time seemed not to be dependent on the material, but strongly depended on the pressurization rate of the system. Due to the constant pressurization rate for the experiments in this thesis the influence was small and should be investigated in future test series.

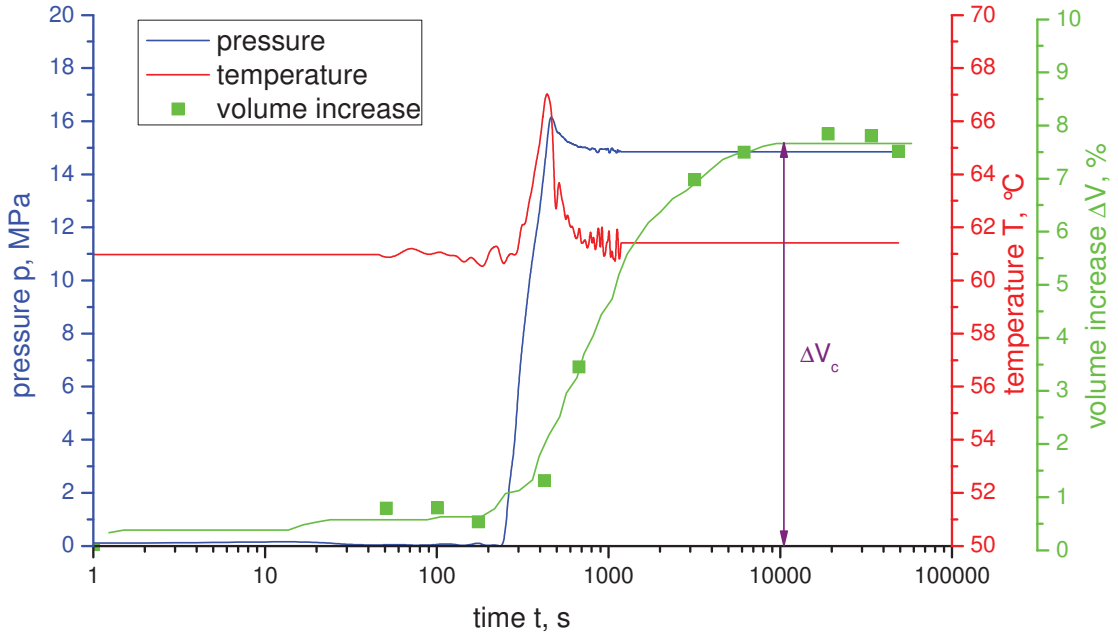

Figure 4.13: Pressure, temperature and volume increase during the compression phase for unconstrained specimens

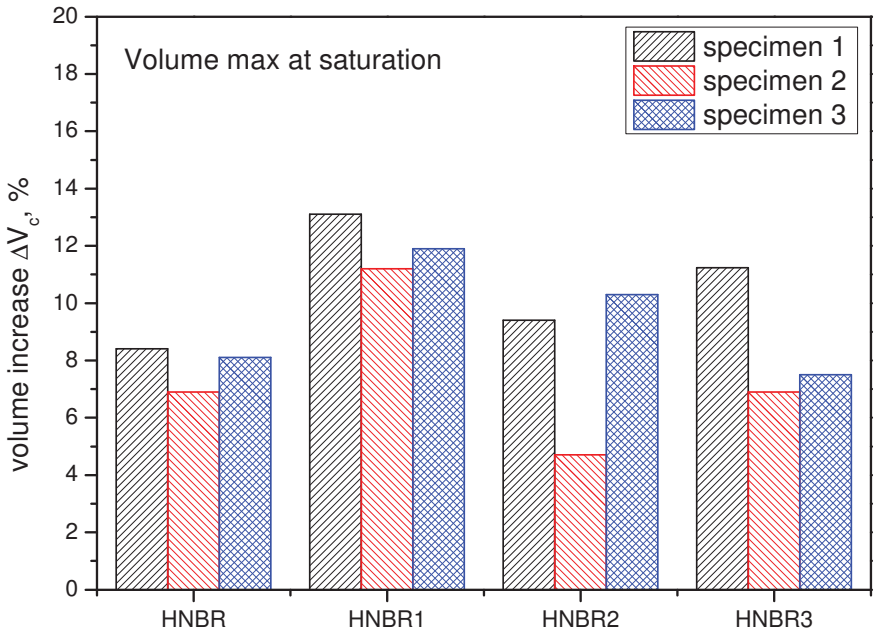

Figure 4.14: Maximum volume increase during pressurization for unconstrained specimens

The volume increase at saturation indicates the amount of stored gas in the material. Therefore Figure 4.14 shows a comparison of the maximum volume increase during pressurization process for all tested materials. The additional filler in HNBR1 resulted in a 50% higher volume increase than in HNBR. The reason of the higher volume increase is based on the filler matrix interface of the vulcanized rubber. With increasing filler content the probability for bad wetted particles increases. Thus, a higher number of microvoids in the material is possible. As discussed in chapter 2 these microvoids were filled with the penetrating gas. Therefore, the volume change increased with the number of microvoids in the material.

With rising acrylonitrile content the maximum volume increase during the compression phase was reduced. This decrease can be explained by the influence of the acrylonitrile content on the permeation properties [Sommer and Röthemeyer, 2006]. The small volume increase for HNBR3 indicates an additional filler (compared to HNBR1). In comparison to HNBR1, a clear difference is observed. This slight increase indicates a much better filler matrix interface for the filler system used in HNBR3.

4.2.1.2 Decompression (incubation of pressure, temperature and volume change)

The decompression phase disturbed the established equilibrium due to the controlled depressurization. As mentioned in chapter 3, a constant decompression rate of 2,25MPa/min was chosen. Because of the adiabatic nature of the process, the temperature decreased (Figure 4.15). The temperature seemed not to be influenced by different materials and was a function of the depressurization rate. As depicted in Figure 4.15, an incubation time Δt_V was observed for the volume change. This threshold goes along with the literature [Briscoe et al., 1994]. The pressure difference between the interior and the exterior increased, thus the internal pressure rose. The material resisted against the volume change, until a specific threshold was reached. Considering Briscoe [Briscoe et al., 1994] this threshold is a function of the pressure difference. When a critical pressure difference is , the material expands. This critical pressure difference is a function of the shear modulus, the surface energy and the initial radius of the void.

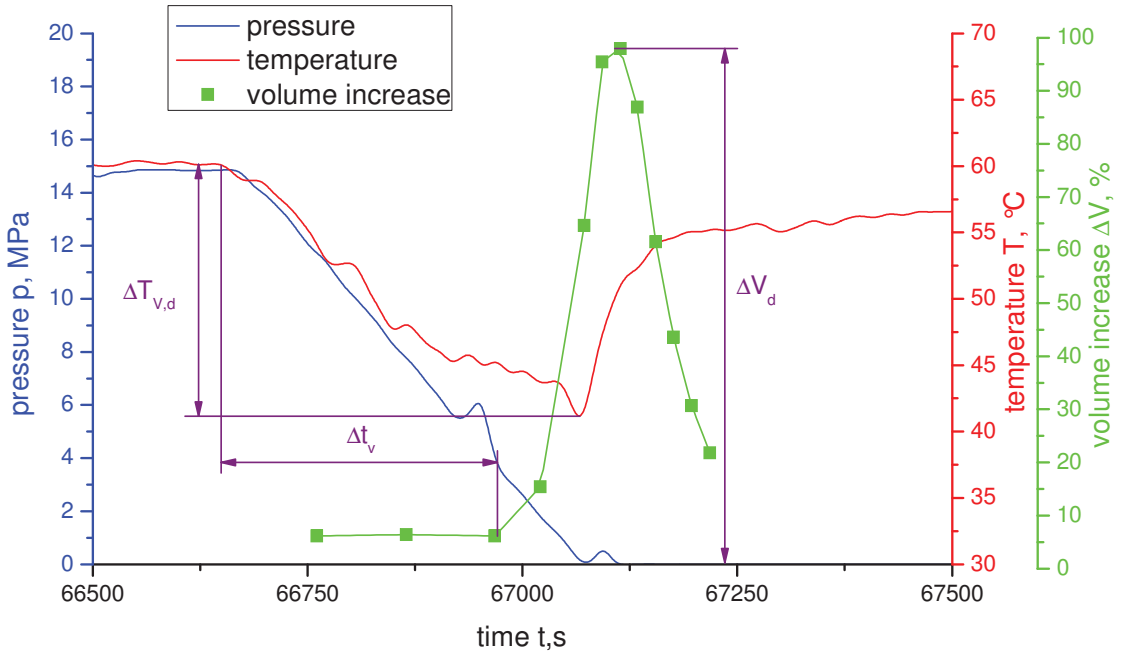

Figure 4.15: Pressure, temperature and volume increase during the decompression phase for unconstrained specimens

Therefore, the incubation time changes for varying decompression rates. Due to the constant decompression rate the incubation time can be used for the comparison of the different materials.

Figure 4.16 shows the summary of the volume increase for the tested materials. As depicted, a strong influence of the additional filler and rising acrylonitrile content was observed. For the additional filler (HNBR1) the maximum volume increase dropped to nearly half of the volume increase of HNBR. This behavior is reasonable, because of a higher failure possibility due to the higher filler content. Furthermore, a small increase for the rising acrylonitrile content due to the decreasing permeation performance of the material was observed [Sommer and Röthemeyer, 2006].

The investigated increase for HNBR3 is a result of the combination of a decrease due to the added filler and an increase because of the rising acrylonitrile content. Due to the better filler matrix interface, as suggested before, and the rising acrylonitrile content fewer bubbles were built during the pressurization process.

Moreover, the permeation performance dropped due to the rising acrylonitrile content. Therefore, the observed volume increase was bigger than for HNBR2.

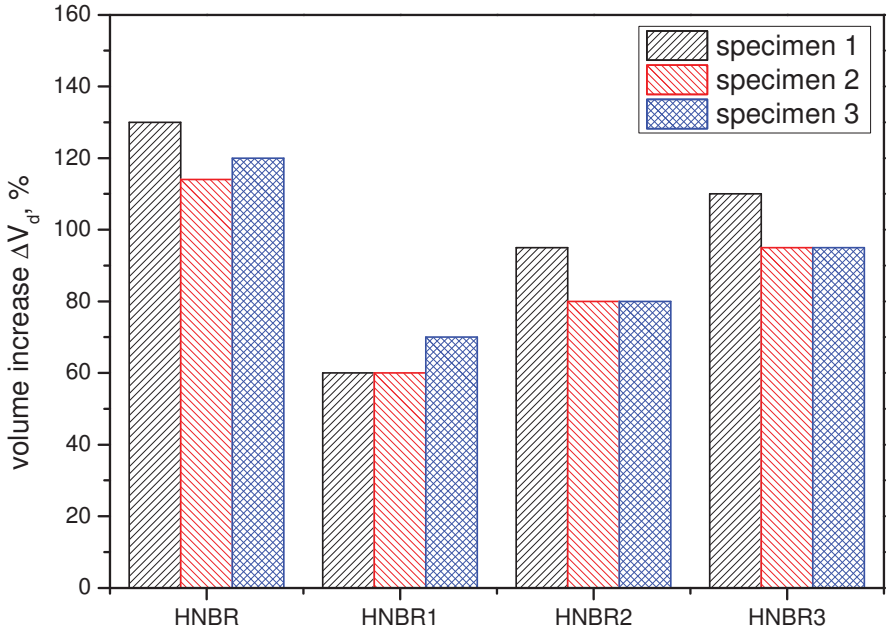

Figure 4.16: Maximum volume increase during decompression for tested materials

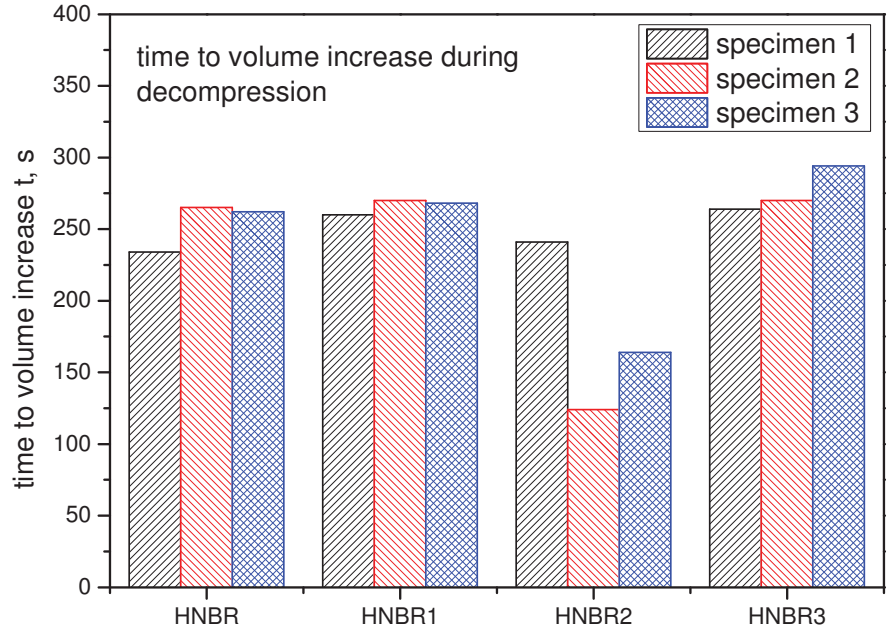

Figure 4.17: Incubation time for unconstrained specimens observed during depressurization

The incubation time for the volume increase during the depressurization process is depicted in Figure 4.17. The differences between HNBR, HNBR1 and HNBR3 do not seem to be mentionable. Because of the softer performance of HNBR2 the drop in comparison to HNBR1 is reasonable. Therefore, the expansion happened earlier.

The temperature decrease for unconstrained specimens during the depressurization process is depicted in Figure 4.18. Due to the small differences between the observed changes, no clear tendency was measured. Thus, the temperature decrease will not be part of the comparison of unconstrained and constrained test set-ups.

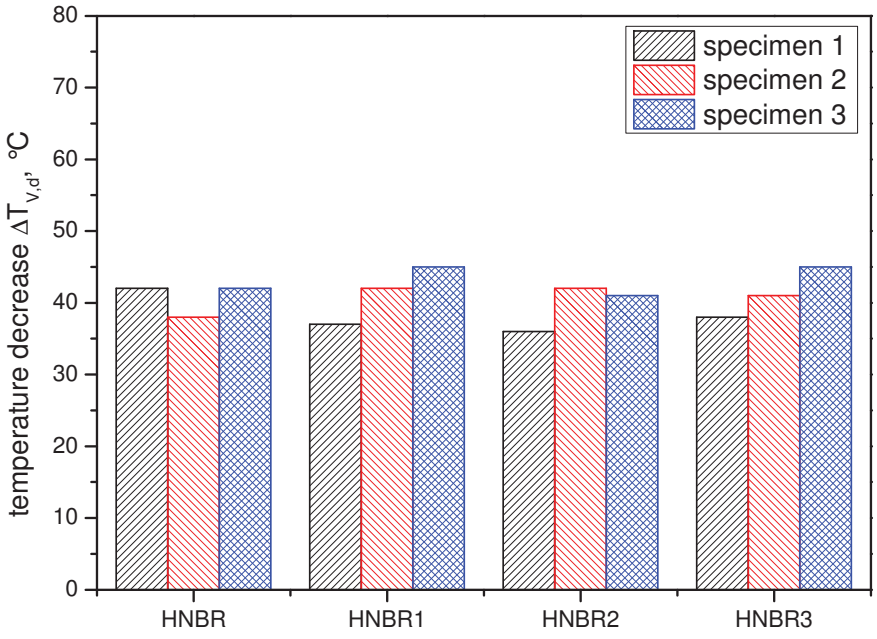

Figure 4.18: Temperature decrease for unconstrained specimens observed during depressurization

4.2.2 Constrained

The implementation for the constrained test set-up will be discussed as a two step process, similar to the unconstrained measurements. Due to the volume change induced by the pressurization process a change of the uniaxial expansion force was measured.

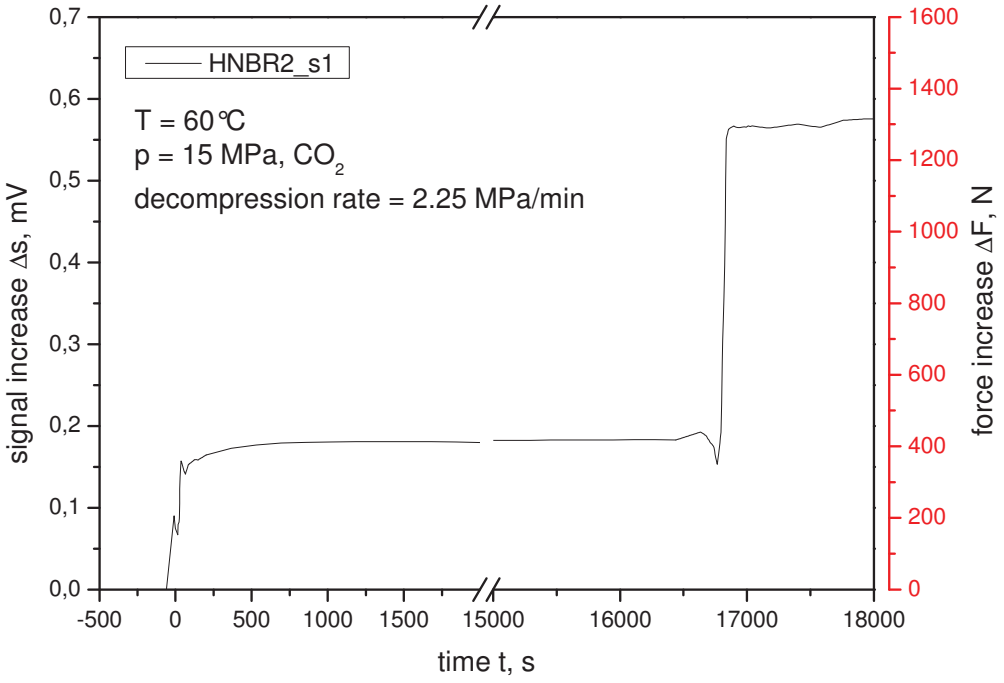

Figure 4.19: Observed force increase for the compression and decompression phase

To get an impression of the investigated force change for the compression and decompression phase, Figure 4.19 shows a representative measurement for tests with a constrained test set-up.

4.2.2.1 Compression (expansion, relaxation, saturation (ΔF_c))

Because of similar test conditions in terms of temperature and pressure, a similar behavior was observed as for unconstrained experiments. The higher metallic mass of the constrained test set-up acts as a small furnace and the temperature reaches the equilibrium faster after the pressurization process.

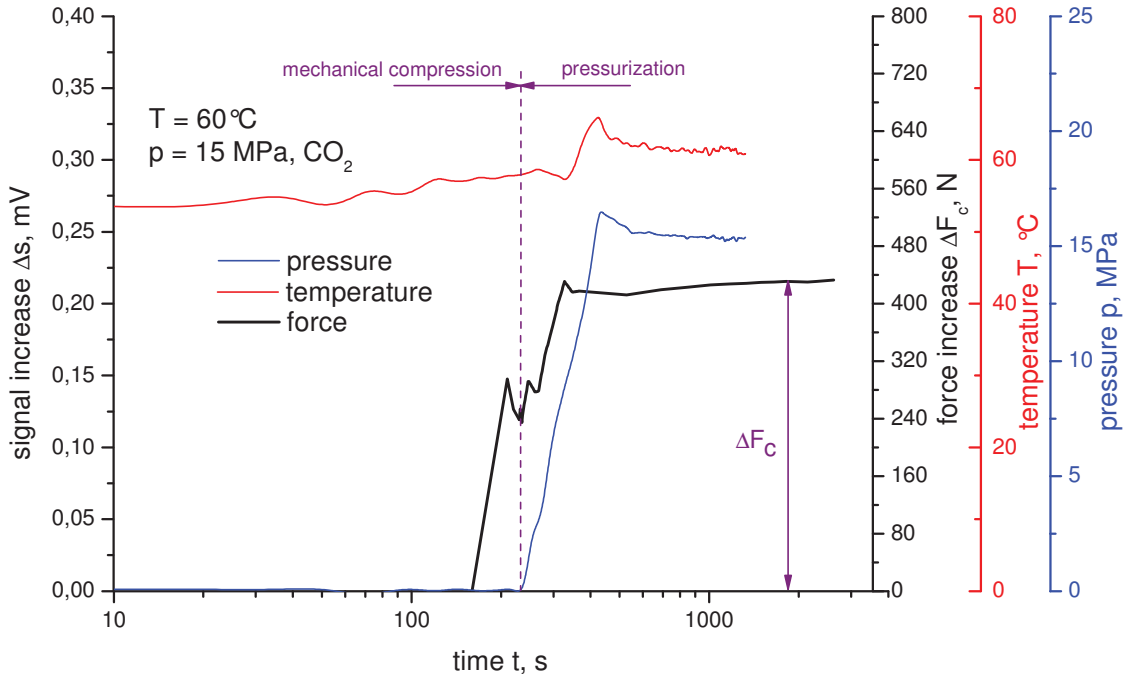

Figure 4.20: Pressure, temperature and force increase during the compression phase for constrained specimens

As depicted in Figure 4.20 the material was preconstrained to a value of 25% by the constrained test set-up. Thus, first a relaxation process of the material was observed. With the start of the pressurization process the force increased and reached a maximum at the end of the pressurization phase. After this maximum, a first decrease of the force was induced. This first decrease can be explained by a relaxation process of the material. With (rising) time the material started the volume change due to the penetration of the gas. Therefore the force change overtook the relaxation process and reached equilibrium with stabilised conditions. Further investigations are necessary to explain the whole change of the force. The maximum force reached during the pressurization process was used for the comparison of the materials.

As depicted in Figure 4.21 no clear tendency was reached for the comparison of the different materials. Further experiments are necessary to find a connection to the rapid gas decompression performance and to suggest in which way the increase of the force influences the material performance.

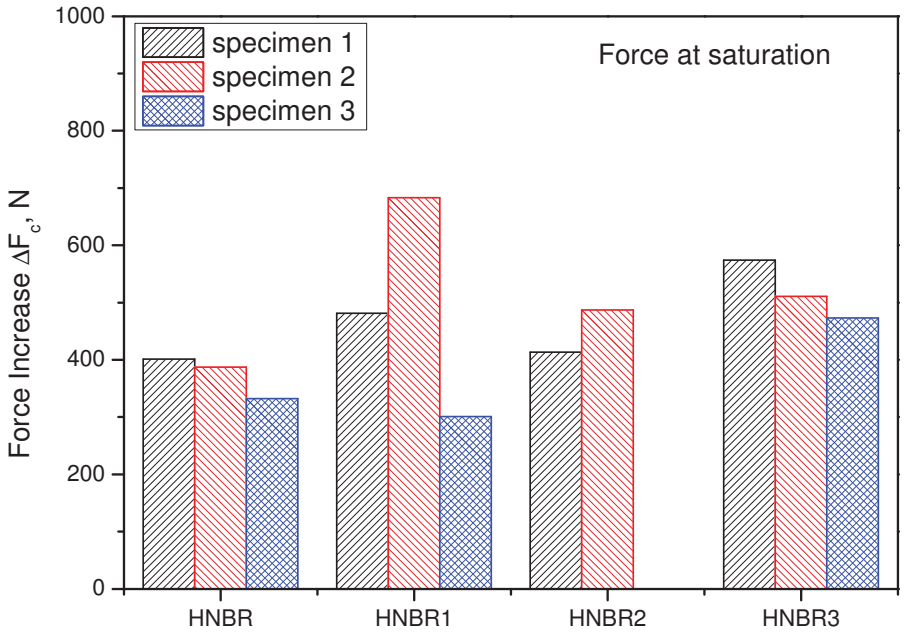

Figure 4.21: Maximum force increase during pressurization for constrained specimens

4.2.2.2 Decompression (volume change, incubation of pressure, temperature and force change)

Due to the controlled depressurization, the decompression phase disturbed the established equilibrium. To provide comparable results the same decompression rate as for the unconstrained measurements, 2.25MPa/min, was used.

Because of the nearly adiabatic process the temperature decreased (Figure 4.22). Concerning the higher metallic mass in the vessel a lower temperature decrease than for unconstrained experiments was observed. The temperature drop investigated during the depressurization seemed independent from the used material. Thus the temperature decrease is only connected to the used decompression rate. Furthermore, a specific incubation time was observed for the increase of the force. This incubation time seemed to be material dependent and due to the constant test parameters this time span was used for the comparison of the different materials and test set-ups. Moreover, also the maximum observed force increase was material dependent and used to better understand the

performance of the different materials. The force signal after the maximum force can not be discussed without further investigations.

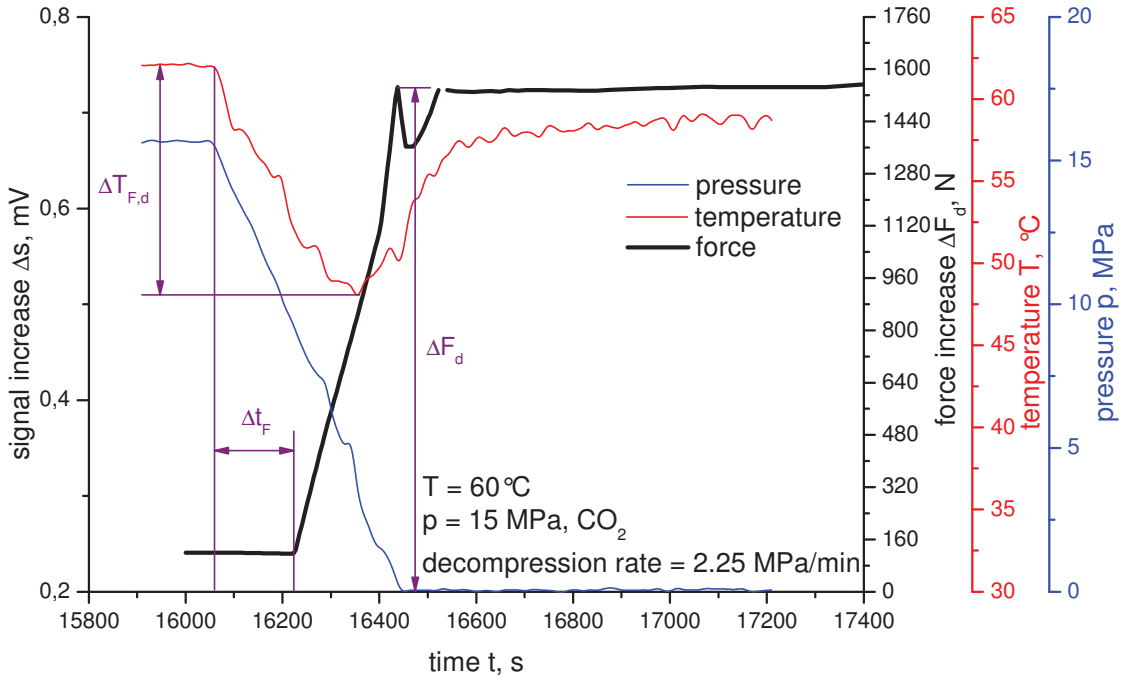

Figure 4.22: Pressure, temperature and force increase during the decompression phase for constrained specimens

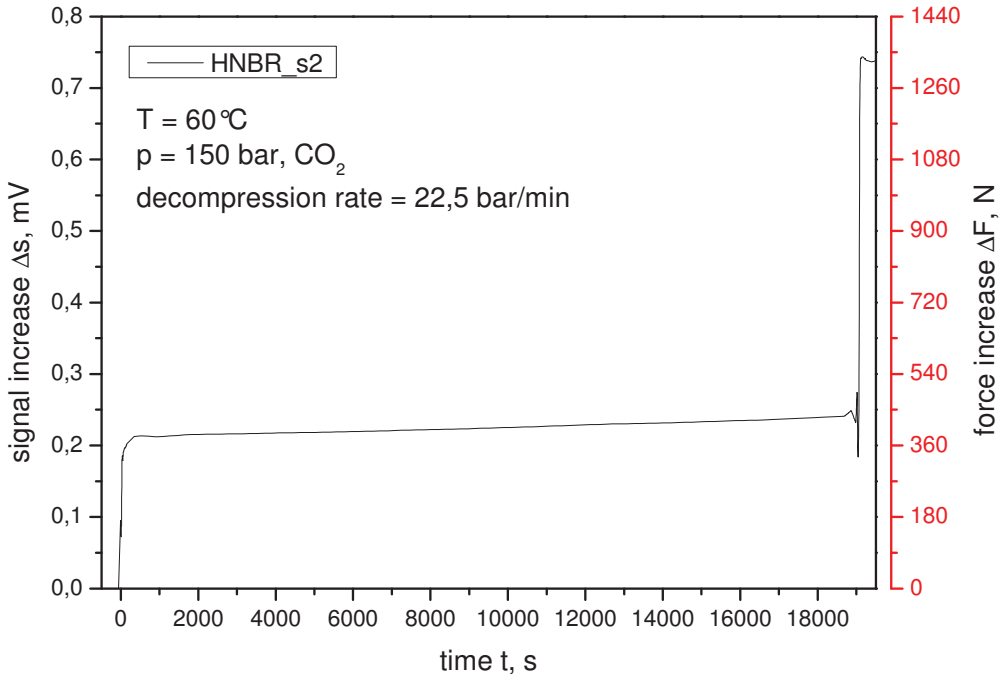

Figure 4.23: Signal and force increase for HNBR under constrained conditions

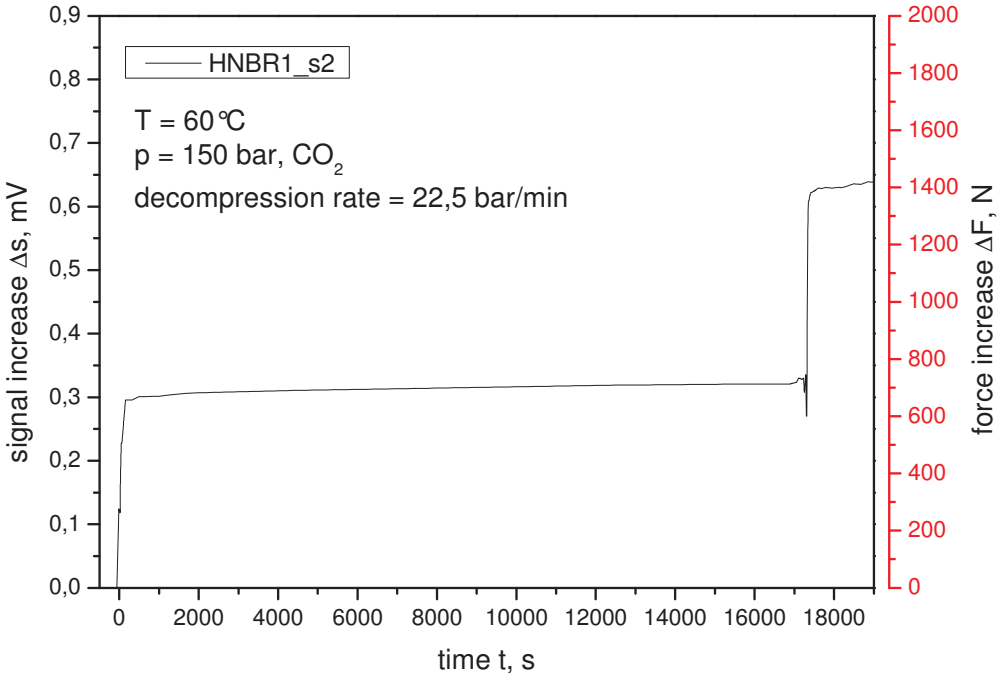

Figure 4.24: Signal and force increase for HNBR1 under constrained conditions

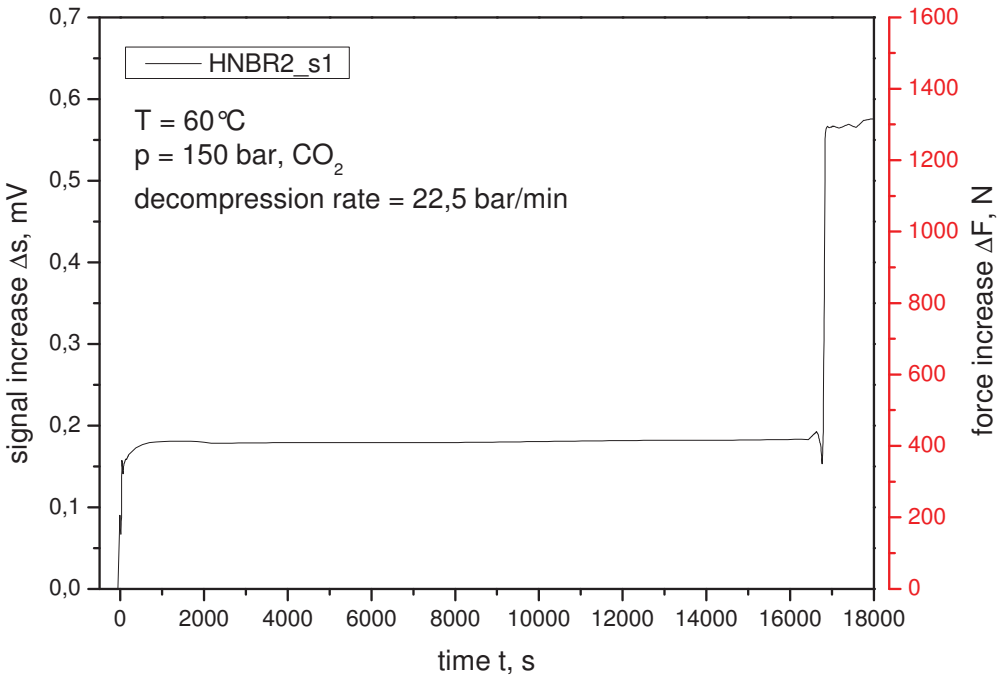

Figure 4.25: Signal and force increase for HNBR2 under constrained conditions

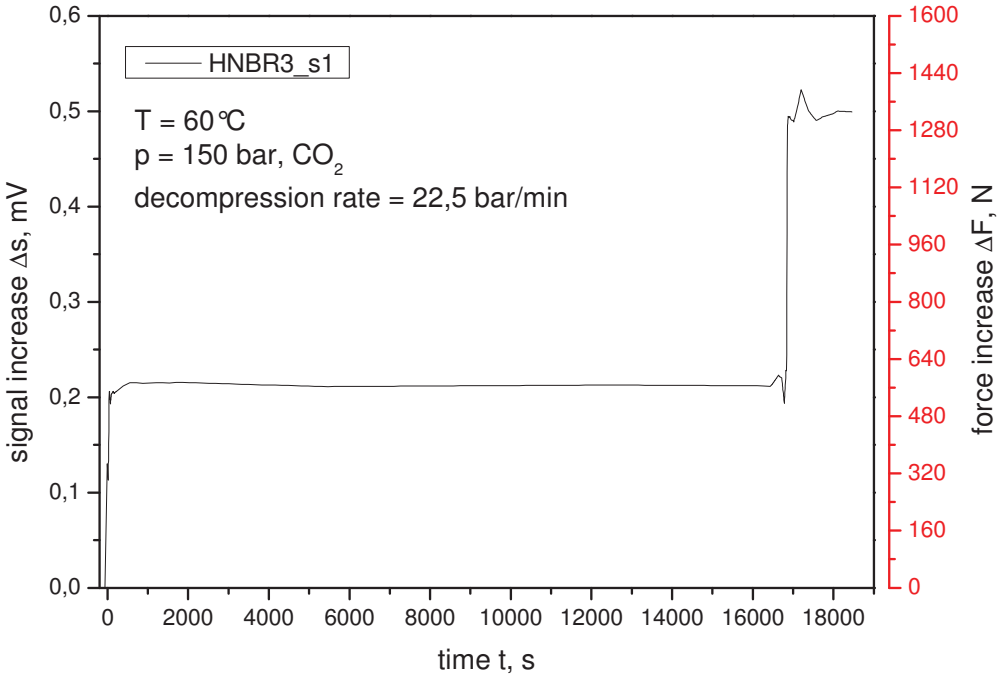

Figure 4.26: Signal and force increase for HNBR3 under constrained conditions

Figure 4.23 to Figure 4.26 show a typical constrained measurement for all 4 tested materials. In Figure 4.27 the maximum force increase during depressurization is depicted. The results for HNBR and HNBR1 go along with the observed behavior of the volume change. Due to the smaller volume change of filled vulcanised rubber the force was reduced for the additional filler. With rising acrylonitrile content the force increased. Because of the softer material performance, observed during the dynamic mechanical characterization HNBR2 also acts softer than HNBR1 in the constrained measurements. The softer behavior results in a bigger volume increase due to the lower force between the polymer chains. Therefore the material expanded easier and the force accelerated. HNBR3 showed a similar force increase in comparison to HNBR2.

Because of the changed filler system and the higher acrylonitrile content no suggestion can be made for the volume increase of the material. To discuss the force increase during depressurization for HNBR3 further materials should be investigated.

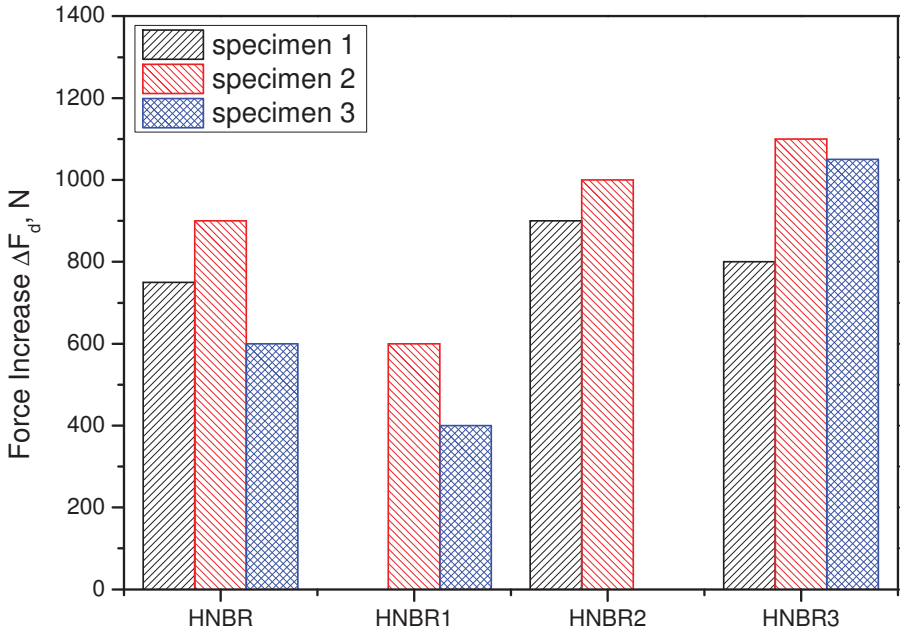

Figure 4.27: Maximum force increase during decompression for tested materials

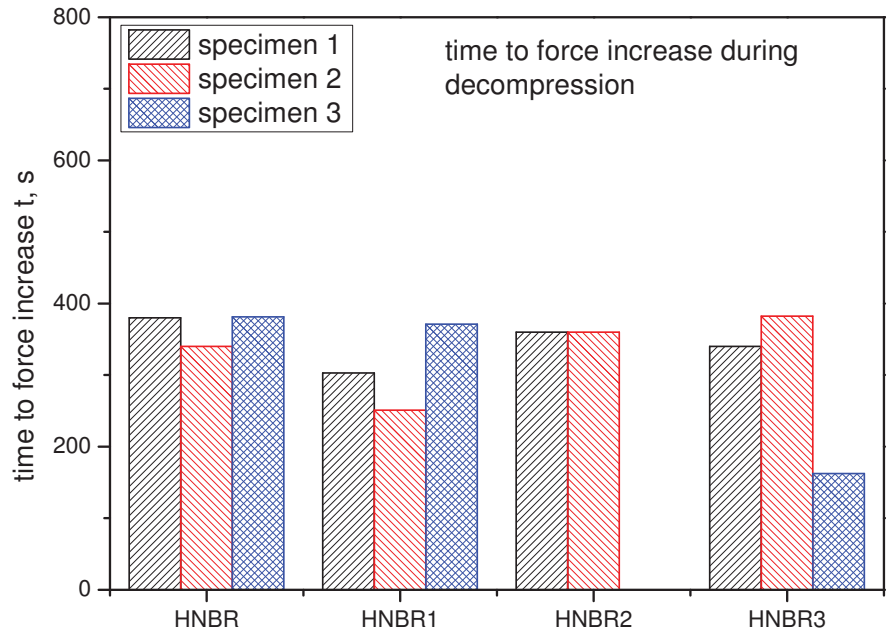

Figure 4.28: Incubation time for constrained specimens observed during depressurization

The incubation time for constrained specimens observed during depressurization is depicted in Figure 4.28. A decrease of the incubation time is investigated for the additional filler. Due to the lower filler content, a better polymer chain movement was observed for HNBR. With increasing filler content this movement was restricted by the filler particles. This restriction resulted in a decreasing incubation time. As mentioned, HNBR2 shows a softer performance than HNBR1. Because of the softer material performance the force built up later, resulting in an increasing incubation time. Due to the higher acrylonitrile content and the other filler system, HNBR3 also shows a complex behavior for this incubation time. To discuss this material, further experiments are necessary.The temperature decrease for constrained specimens during the depressurization process is depicted in Figure 4.29. Due to the small differences between the observed changes, no clear tendency was measured. Thus, the temperature decrease will not be part of the comparison of the unconstrained and constrained test set-ups.

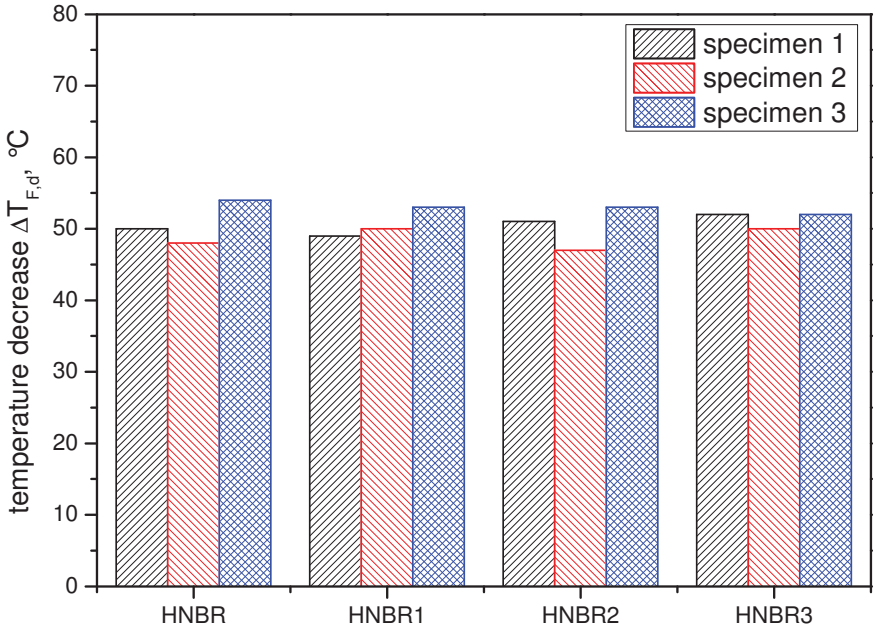

Figure 4.29: Temperature decrease for constrained specimens observed during depressurization

4.2.3 Comparison of unconstrained and constrained measurements

For the comparison of unconstrained and constrained measurements several factors were used. Chapter 3 gives an overview of these factors. HNBR3 will not be used for the comparison because of the change of two variables (acrylonitrile content and filler system). Therefore, a clear separation of both effects is impossible. The other three materials showed a clear correlation and will therefore be deal with. As depicted in Figure 4.30 two factors were investigated. The filler factor between HNBR and HNBR1 reflects the influence of the filler on the volume/force increase and the incubation time. The second factor, the acrylonitrile factor represents the influence of the acrylonitrile content on the performance of the materials.

Figure 4.30: Relation between the experimental materials and the filler/ACN factor

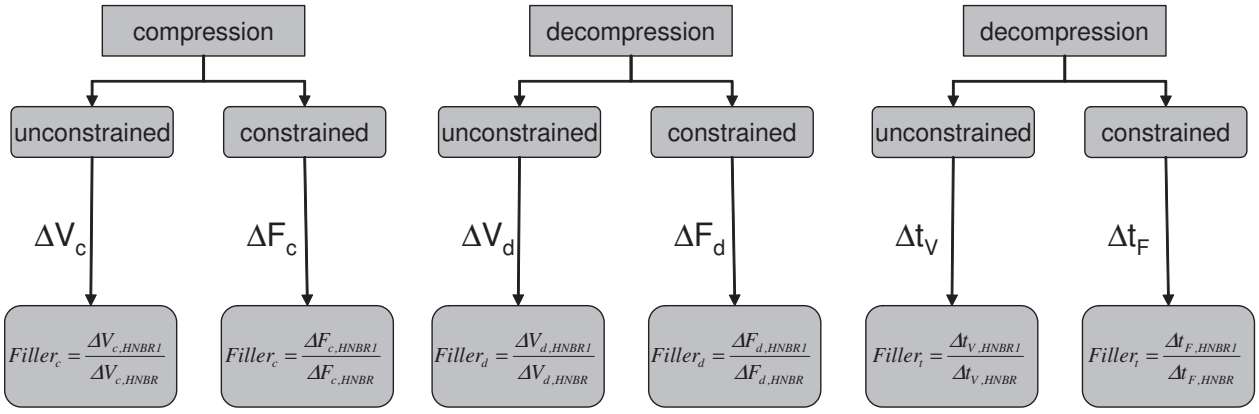

Figure 4.31: Overview of the used parameters to rank the material

Figure 4.31 shows an overview of the used filler factors and their connection to the measured values. During the pressurization phase, the volume/force increases, indicated by a filler factor value higher than 1 (Figure 4.32). This increase was investigated because of the change in the filler matrix interface due to the additional filler. Therefore, the volume and the force rose during the compression

phase. For the decompression of the established equilibrium a drop for the volume change and for the force was observed. The added filler results in a bigger failure possibility. Therefore the volume and the force showed smaller values.

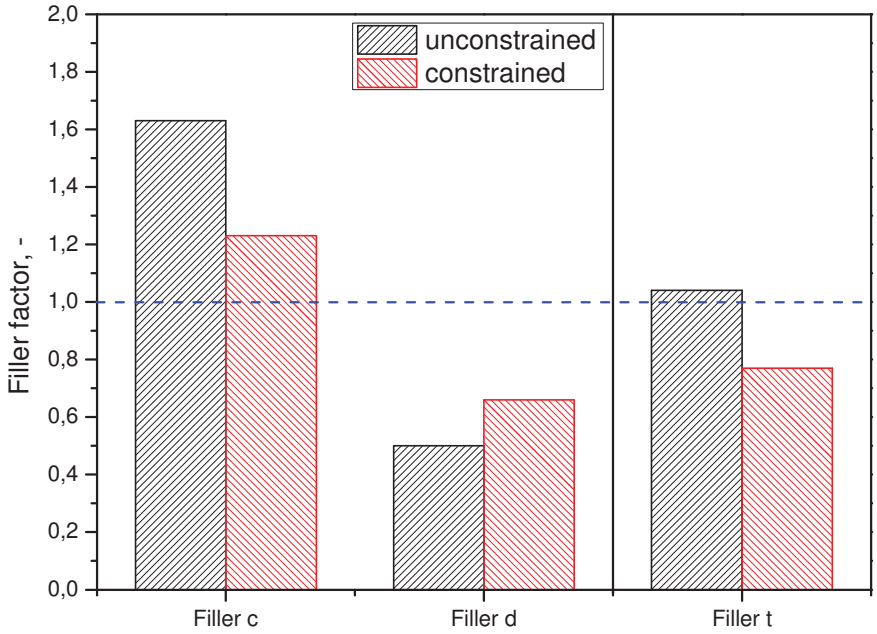

Figure 4.32: Influence of the filler on compression, decompression phase and on the incubation time

No influence of the additional filler on the incubation time was found for the volume change. Due to the increasing filler content the movement of the polymer chains was restricted by the filler particles. Hence, the free expansion of the polymer chains decreased. Therefore, the stress in the material was produced earlier than for lower filled systems. This limitation doesn't affect the incubation time up to the volume increase (Filler t, unconstrained), but influences the incubation time until the force increase begins (Filler t, constrained).

In Figure 4.33 the effect of rising acrylonitrile content is depicted. Due to the decreasing permeability [Sommer and Röthemeyer, 2006] with rising acrylonitrile content the ACN factor for the compression phase decreased. The drop of the force during the compression phase correlated with the smaller volume increase. For the depressurization phase a higher volume increase was investigated with

rising acrylonitrile content. Because of the softer material performance the force within the material was smaller and thus resulted in a higher expansion. Furthermore, a faster increase of the volume change during the decompression was observed for HNBR2. Therefore a higher force for constrained measurements was reached.

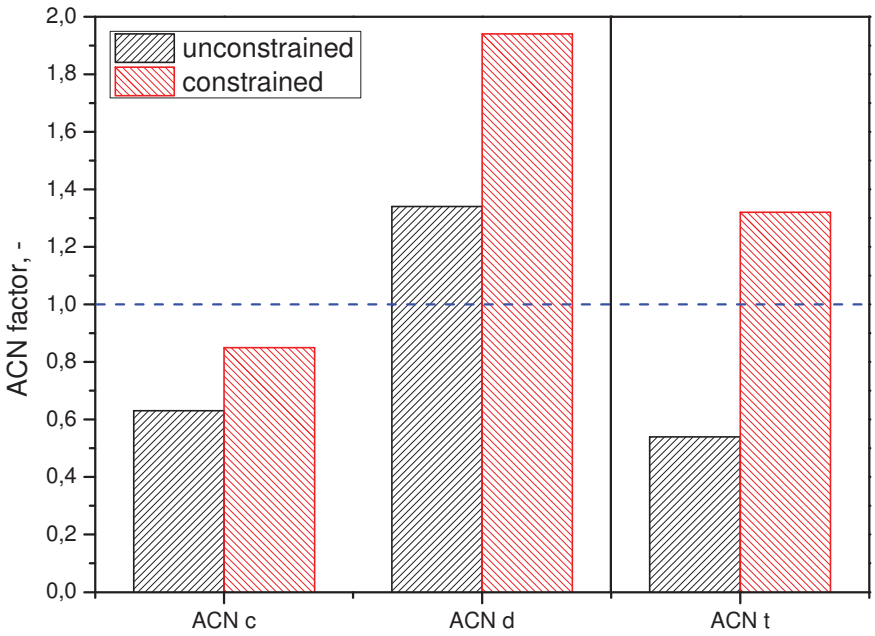

Figure 4.33: Influence of ACN on compression, decompression phase and on the incubation time

The incubation time correlated with the observed performance of the material. With decreasing hardness the unconstrained volume expansion was faster, but the force built up later.

5 CONCLUSIONS

Based on the experimental results described above some general conclusions may be drawn:

Related to method development:

- In comparison to the conventional characterization of the rapid gas decompression behavior the additional instrumented constrained test set-up increases the complexity of the experiment and hence the characterization of the material. However, to support novel test standards, the determination of all influencing parameters and parameter combinations on the material behavior is necessary.

- The results of both the unconstrained and the constrained tests can later be used for supporting the numerical simulation of the RGD process

- To reduce the influence of the test set-up on the recorded material curves, an adaptation of the autoclave is needed. Moreover, additional test set-ups have to be built to characterize the material properties (e.g. tensile, compression, dynamic properties) under high temperatures and exposure of high pressure gas.

Related to the material characterization and material behavior under RGD conditions:

- Due to the additional filler a volume and force increase is reached for the pressurization phase.

- Furthermore, the rising acrylonitrile content shows a decrease for the volume and force change during the pressurization process.

- For the decompression process the volume and force drop to smaller values with additional filler.

- Moreover, a higher volume and force increase is realized with rising acrylonitrile content.

- The incubation time for constrained measurements decreases with additional filler.

- However, the additional filler has no influence on the incubation time for the volume change.

- Additionally, a good correlation of the incubation time and volume change is observed.

As mentioned in chapter 2, the Young's modulus and the overall stiffness of the elastomers (slope of the stress-strain curve) is one of the most important values regarding RGD resistance. The instrumented tests allow for the determination of both the volume increase of the test specimen under unconstrained conditions and the reaction forces under constrain conditions.

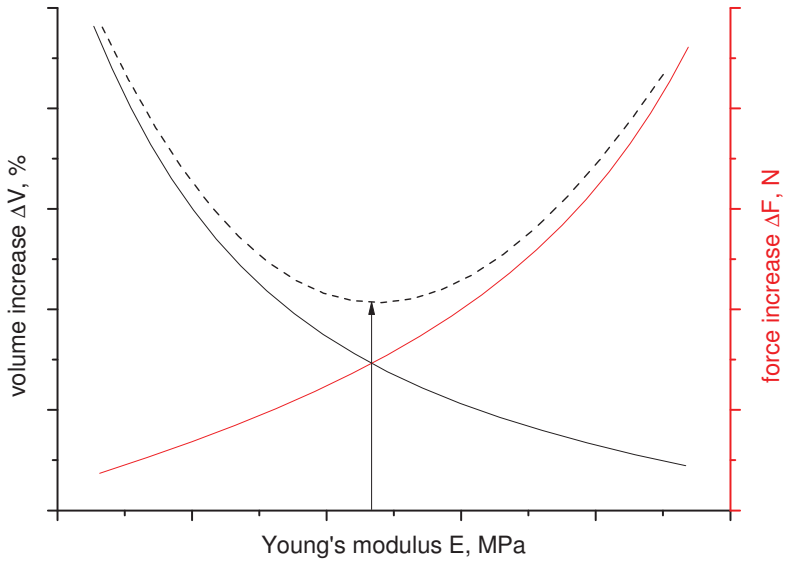

Figure 5.1: Schematic representation of the Young's modulus dependence of the volume increase and force increase

Based on these tendencies a simple model for describing the relationship between the volume increase, the force increase and the Young's modulus is established. The schematic representation of this model is depicted in Figure 5.1. While the volume change assumed to decrease with increasing modulus, the higher Young's modulus results in higher force values. Both curves cross each other providing a point, where the volume increase and the force increase are at a local minimum. This point describes a material with optimal Young's modulus providing the best material performance for the application needed. To verify this theory, further investigations are necessary and different problems have to be investigated:

- Material development problem; high influence of the acrylonitrile content and the filler system, the volume change decreases with rising acrylonitrile content,

- Mechanical problem, small strain (<15%) during the compression phase and high strain values (>100%) during the decompression phase, the small strain Young`s modulus values are not sufficient to describe the process, the material must be stiff enough at high strains too.

- Ambient conditions problem, influence of pressure, different gases and temperature.

- Due to the reduced elasticity (flexibility, deformability) the application of too stiff materials is limited. The seal must fulfil its sealing function too.

- In this simplified model, there is no distinction between the compression (gas diffusion and solution) and the decompression (the ability of the solved gas to move outside of the material) processes. An improved model should contain of the balance analysis of both processes.

Finally, in addition to the deformation analysis, for a better understanding of the crack initiation and growth process fracture mechanic experiments have to be implemented.

6 BIBLIOGRAPHY

Amerongen G.J. (1964). Rubber Chem. Tech. 37, 1065.

Andrews E.H., Stevenson A. (1978). J. Mater. Sci. **13**, 1680.

Briscoe B.J., Gritsis D., Liatsis D. (1992). Phil. Trans. R. Soc. London. A **A339**, 497.

Briscoe B.J., Savvas T., Kelly C.T. (1994). Rubber Chem. Tech. **67**, 384.

Briscoe B.J., Zakaria S. (1990). J. Mater. Sci. **25**, 3017.

Briscoe B.J., Zakaria S. (1992). J. Polym. Sci. Part B: Polym. Phys. Ed. **30**, 959.

Briscoe B.J., Zakaria S. (1990). Polymer **31**, 440.

Briscoe B.J., Zakaria S. (1990). Polymer Test. **9**, 103.

Campion R.P. (1990). Cell Polym. **9**, 206.

Carpenter A.S., Twiss D.F. (1940). Ind. Eng. Chem., Anal. Ed. **12**, 99.

Cohen D.S., White A.B. jr. (1991). SIAM J. Appl. Math. **51** (2), 472.

Cohen D.S., White A.B. jr., Witelski T.P. (1995). SIAM J. Appl. Math. **55** (2), 348.

Crank J. (1975). In "The Mathematics of Diffusion", (Clarendon Press), 2nd Edition, pp. 254-257, Oxford.

Crank J., Park G.S. (1968). In "Diffusion in Polymers", (Crank J., Park G.S., ed.), pp.1-39, Academic Press, London.

Derham C.J., Thomson B. (2003). In Proc. „Oilfield Engineering with Polymers 2003", Paper No 1,Materials Engineering Research Laboratory Limited, Hertford, UK.

DIN 53504: Testing of rubber – determination of tensile strength at break, tensile stress at yield, elongation at break and stress values in a tensile test. Deutsches Institut für Normung e.V., Berlin, DIN 53504:2009-10.

Domellen J.A.W., Schrauwen B.A.G., Breemen L.C.A., Govaert L.E. (2004). J. Polym. Sci. Part B: Polym. Phys. **42**, 2983.

Ender D.H. (1986). Chemtech. **16**, 52.

Fleming G.K., Koros W.J. (1986). Macromolecules **19**, 2285.

Fujita H. (1968). In "Diffusion in Polymers", (Crank J., Park G.S., ed.), pp.75-105, Academic Press, London.

Gastl S. (in Prog.). „Characterization and Simulation of the time dependent behaviour of particle filled polypropylen compounds by DIGIMAT“, Master Thesis, Institute of Materials Science and Testing of Plastics, University of Leoben, Austria.

Gee G. (1947). Q. Rev. Chem. Soc. **1**, 265.

Gent A.N. (1980). J. Mater. Sci. **15**, 2884.

Gent A.N. (1990). Rubber Chem. Tech. **63**, G49.

Gent A.N., Lindley P.B. (1958). R. Soc. London Ser. A **A249**, 195.

Gent A.N., Tompkins D.A. (1969). J. Appl. Phys. **40**, 2520.

Gent A.N., Tompkins D.A. (1969). J. Polym. Sci. Part B: Polym. Phys. Ed.(A-2) **7**, 1483.

Gent A.N., Park B. (1984). J. Mater. Sci. **19**, 1947.

Gent A.N., Wang C. (1991). J. Mater. Sci. **26**, 3392.

Griffiths A.D. (1985). In Proc. “Discussion Forum and Exhibition on “Offshore Engineering with Elastomers”, Paper No 20, Plast. Rubber Inst., Aberdeen, Scotland.

Hertz D.L. jr. (1996). In Proc. “ERG Fall Technical Meeting”, Seals Eastern Inc., Houston, Texas.

Hou H.S., Abeyaratne R. (1992). J. Mech. Phys. Solids **40**, 571.

James Walker (2009). In “Sealing Guide for the Oil & Gas Industry”, (James Walker, ed.), p. 1-34, James Walker, Aberdeen, UK.

Jerabek M. (2009). “Advanced Characterization of the Tensile and Compressive Behavior of PP and PP Composites”, Ph.D. Thesis, Institute of Materials Science and Testing of Plastics, University of Leoben, Austria.

Jerabek M., Major Z., Lang R.W. (2010). Polymer Test. **29**, Issue 3, 302.

Jordan S.M., Koros W.J. (1990). J. Polym. Sci. Part B: Polym. Phys. **28**, 795.

Kadir A., Thomas A.G. (1979). In “Elastomers: Criteria for Engineering desing”, (Hepburn C., Reynolds J.W., Eds), ch. 5, p. 67, Applied Science Publishers, London.

Kamiya Y., Hirose T., Mizoguchi K., Naito Y. (1986). J. Polym. Sci. Part B: Polym. Phys. **24**, 1525.

Lake G.J., Samsuri A., Teo S.C., Vaja J. (1991). Polymer **32**, 2963.

Lederer K. (2006). „Characterization of Rapid Gas Decompression Behavior of Pressurized Elastomer Seals“, Master Thesis, Institute of Materials Science and Testing of Plastics, University of Leoben, Austria.

Liatsis D. (1989). “Gas Induced Rupture of Elastomers”, Ph.D. Thesis, Imperial College, University of London, GB.

Lindsey G.H. (1967). J. Appl. Phys. **38**, 12.

Major Z., Lang R.W. (2010). Engineering Failure Analysis **17**, Issue 3, 701.

Melikhova N.A., Reitlinger S.A., Kuzina E.N. (1959). Sov. Rubber Technol. **18**, 34.

Nagdi K. (1993). In “Rubber as an engineering material: guideline for users”, (Nagdi K., Eds), Hanser Publ., Munich, Vienna, New York, Barcelona.

NACE Standard Test Method: Evaluating Elastomeric Materials in Carbon Dioxide Decompression Environments. Nace International, Houston, Texas, TM0192-2003.

NORSOK Standard: Qualification of non-metallic sealing materials and manufacturers. Norwegian Technology Centre, Oslo, Norway, M-710, Rev. 2, October 2001.

Schmitt W. (1987). In “Kunststoffe und Elastomere in der Dichtungstechnik“, (Schmitt W., Eds), Kohlhammer Verlag, Stuttgart, Berlin, Köln, Mainz.

Shah V.M., Hardy B.J., Stern S.A. (1986). J. Polym. Sci. Part B: Polym. Phys. **24**, 2033.

Smallwood W.M. (1944). H. Appl. Phys. **151**, 758.

Sommer F., Röthemeyer F. (2006). In „Kautschuktechnologie“, (Sommer F., Röthemeyer F., Eds), ch. 2, p. 107-122, ch. 3, p. 231-243, Carl Hanser, Munich.

Stern S.A., Mullhaupt J.T., Gareis P.J. (1969). AlChE J. **15**, 64.

Stern S.A., Shiah S.P. (1981). Mol. Pharmacol. **19**, 56.

Stern S.A., Shah V.M., Hardy B.J. (1987). J. Polym. Sci. Part B: Polym. Phys. **25**, 1263.

Stevenson and Morgan (1995). Rubber Chem. Tech. **68**. 197.

Stewart C.W. (1970). J. Polym. Sci. Polym. Phys. Ed. (A-2) **8**, 937.

Tanioka A. et al (1982). J. Polym. Sci. Part B: Polym. Phys. Ed. **20**, 2197.

Vezer S.T. (in Prog.). “Characterization and Modelling of the Fretting Fatigue Behaviour of Elastomers”, Ph.D. Thesis, Institute of Materials Science and Testing of Plastics, University of Leoben, Austria.

Vorotnikov D.A. (2009). J. Differential Equations **246**, 1038.

Willimas M.L., Schapery R.A. (1965). Intern. J. Fract. Mech. **1**, 64.

Zakaria S. (1990). “Gas-Polymer Interactions at High Pressures”, Ph.D. Thesis, Imperial College, University of London, UK.

7 APPENDICES

7.1 List of tables

7.2 Table of figures